Supporting Information for: Efficient Parametrization of Force Field for The Quantitative Prediction of Physical Properties of Ionic Liquid Electrolytes

Nikhil V. S. Avula,[†] Anwesa Karmakar,[†] Rahul Kumar,[†,‡] and Sundaram Balasubramanian[*,†]

[†]*Chemistry and Physics of Materials Unit, Jawaharlal Nehru Centre for Advanced Scientific Research, Bangalore 560064, India*

[‡]*Current address: Department of Chemical and Biomolecular Engineering, Tulane University, New Orleans, LA, 70118, USA*

E-mail: bala@jncasr.ac.in

Phone: +91 (80) 2208 2808. Fax: +91 (80) 2208 2766

Contents

S1 Force Field Nomenclature

GAFF uses a simple functional form, often called the "class I" model, to compute the total potential energy as shown in equation S1.[1] In this framework, bonds, angles, dihedrals, and impropers constitute the bonded interactions that act within a molecule while Lennard-Jones (LJ) and Coulomb interactions constitute the non-bonded interactions that act between molecules (and also between atoms within a molecule separated by more than 3 bonds).

$$\begin{aligned} E = & \sum_{bonds} k_b(r - r_0)^2 + \sum_{angles} k_\theta(\theta - \theta_0)^2 \\ & + \sum_{dihedrals} k_\phi(1 + cos(n\phi - \delta_\phi)) + \sum_{impropers} k_\psi(1 + cos(n\psi - \delta_\psi)) \\ & + \sum_{i=1}^{N-1} \sum_{j>i}^{N} \left\{ 4\epsilon_{ij} \left[\left(\frac{\sigma_{ij}}{r_{ij}} \right)^{12} - \left(\frac{\sigma_{ij}}{r_{ij}} \right)^{6} \right] + \frac{1}{4\pi\epsilon_0} \frac{q_i q_j}{r_{ij}} \right\} \end{aligned} \tag{S1}$$

S2 Atom Type Nomenclature

The following sections provide the chemical structures, atom type and atom number nomenclature of N,N-diethyl-N-(2-methoxyethyl)-N-methylammonium (DEME) cation, bis-(trifluoromethylsulfonyl)-imide (TFSI) anion and N,N-dimethyl-N-ethyl-N-methoxyethoxyethylammonium ($N_{112,2O2O1}$) cation used in this work. The atom type nomenclature in the refined force field (refinedFF) expands upon the typing scheme of GAFF.[1] Two additional atom types were introduced - *cacn* to differentiate the carbon atoms directly connected to the quarternary nitrogen (n4) from the rest of the carbon atoms and *anc3* to differentiate the carbon atoms in the anion from that of the cation.

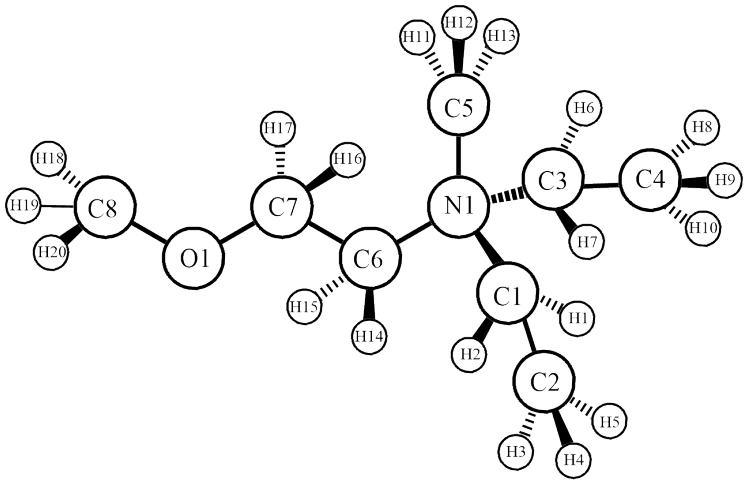

Figure S1: Atom numbering scheme of atoms in DEME cation.

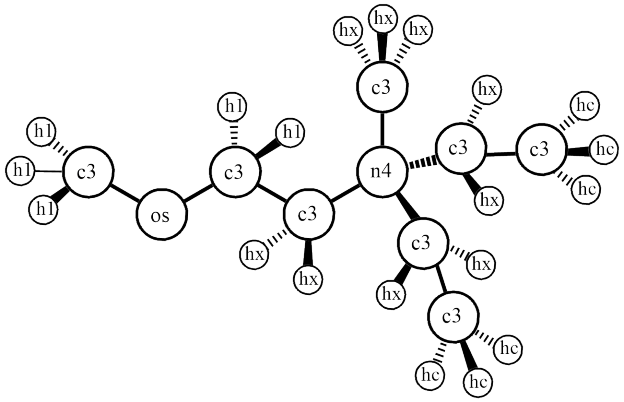

Figure S2: Atom types of atoms in DEME cation in GAFF scheme.

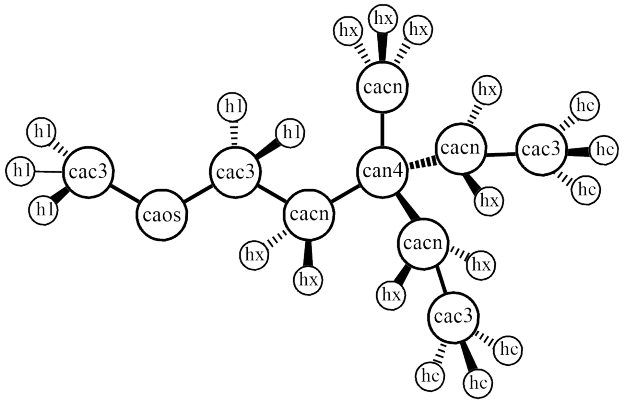

Figure S3: Atom types of atoms in DEME cation in refinedFF scheme.

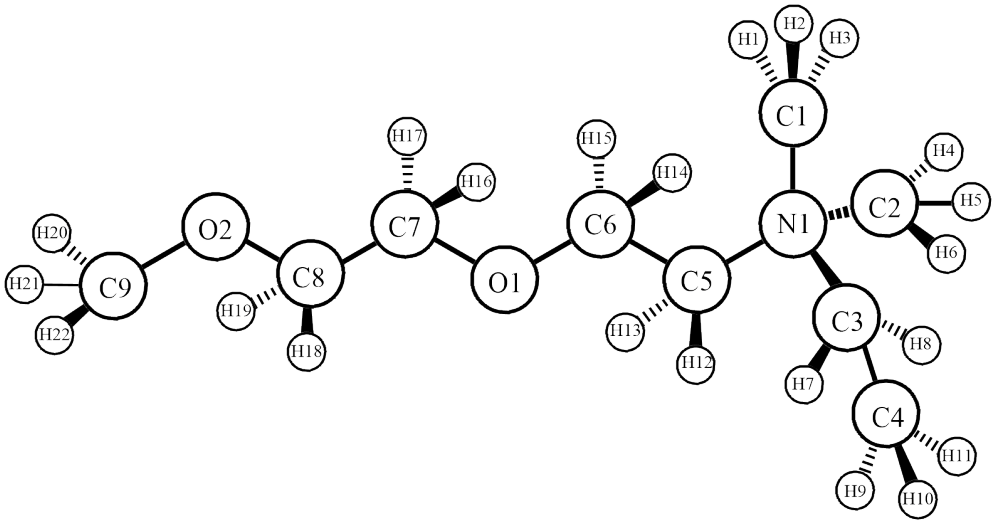

Figure S4: Atom numbering scheme of atoms in $N_{112,2O2O1}$ cation.

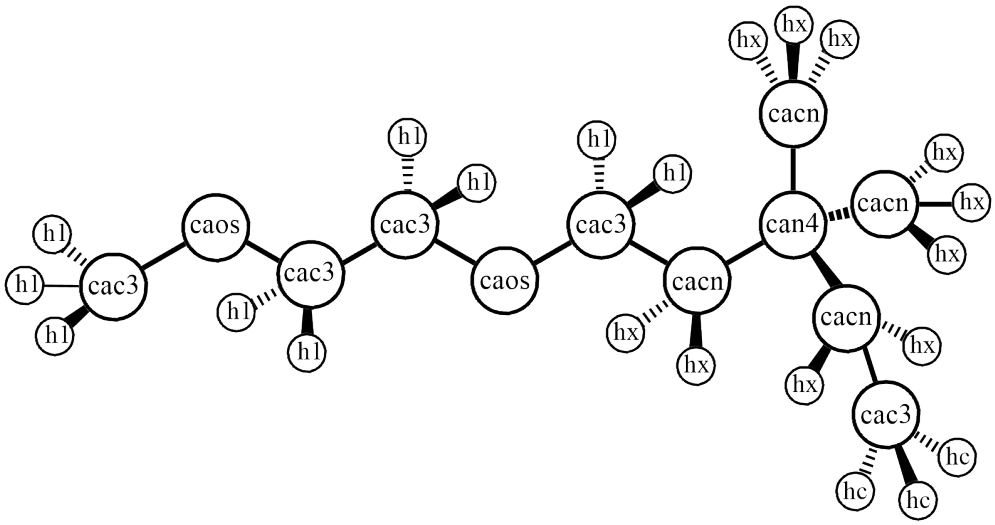

Figure S5: Atom types of atoms in cation in $N_{112,2O2O1}$ refinedFF scheme.

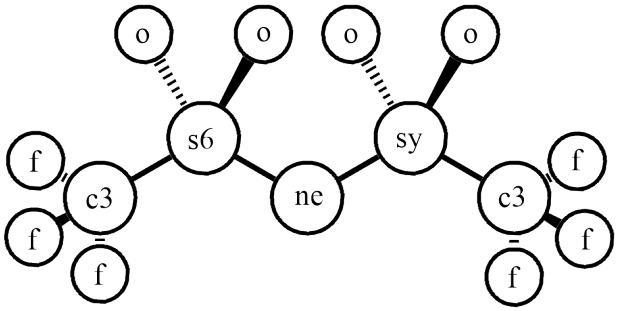

Figure S6: Atom types of atoms in TFSI anion in GAFF scheme.

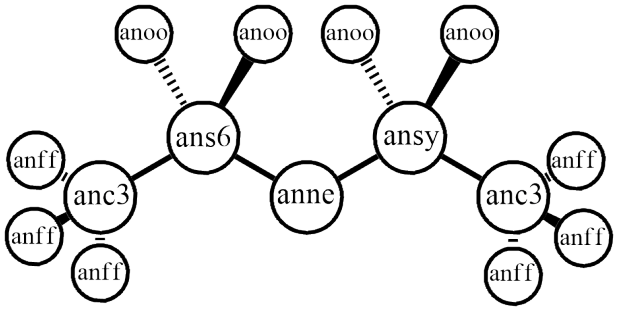

Figure S7: Atom types of atoms in TFSI anion in refinedFF scheme.

S3 Simulation Run Details

Table S1: Simulation run details used to estimate density.

IL system	Force Field	State point	Ion Pairs	NPT (ns)	NVT (ns)	Independent runs
DEME-TFSI	GAFF+1.00*RESP	298K 1bar	128	20	-	1
DEME-TFSI	GAFF+0.90*RESP	298K 1bar	128	20	-	1
DEME-TFSI	GAFF+0.80*RESP	298K 1bar	128	20	-	1
DEME-TFSI	GAFF+DDEC/c6	298K 1bar	128	20	-	1
DEME-TFSI	GAFF+0.70*RESP	298K 1bar	128	20	-	1
DEME-TFSI	GAFF+0.60*RESP	298K 1bar	128	20	-	1
DEME-TFSI	GAFF+0.55*RESP	298K 1bar	128	20	-	1
DEME-TFSI	GAFF+0.50*RESP	298K 1bar	128	20	-	1
DEME-TFSI	LJ pilot runs	298K 1bar	128	20	-	1
DEME-TFSI	refinedFF	298K 1bar	128	20	-	1
DEME-TFSI	refinedFF	303K 1bar	128	20	-	1
DEME-TFSI	refinedFF	313K 1bar	128	20	-	1
DEME-TFSI	refinedFF	323K 1bar	128	20	-	1
DEME-TFSI	refinedFF	333K 1bar	128	20	-	1
DEME-TFSI	refinedFF	343K 1bar	128	20	-	1
DEME-TFSI	refinedFF	353K 1bar	128	20	-	1
$N_{112,2O2O1}$-TFSI	refinedFF	298K 1bar	128	20	-	1
$N_{112,2O2O1}$-TFSI	refinedFF	303K 1bar	128	20	-	1
$N_{112,2O2O1}$-TFSI	refinedFF	313K 1bar	128	20	-	1
$N_{112,2O2O1}$-TFSI	refinedFF	323K 1bar	128	20	-	1
$N_{112,2O2O1}$-TFSI	refinedFF	333K 1bar	128	20	-	1
$N_{112,2O2O1}$-TFSI	refinedFF	343K 1bar	128	20	-	1
$N_{112,2O2O1}$-TFSI	refinedFF	353K 1bar	128	20	-	1

Table S2: Simulation run details used to estimate diffusion coefficients.

IL system	Force Field	State point	Ion Pairs	NPT (ns)	NVT (ns)	Independent runs
DEME-TFSI	GAFF+1.00*RESP	298K 1bar	128	-	100	1
DEME-TFSI	GAFF+0.90*RESP	298K 1bar	128	-	100	1
DEME-TFSI	GAFF+0.80*RESP	298K 1bar	128	-	100	1
DEME-TFSI	GAFF+DDEC/c6	298K 1bar	128	-	100	1
DEME-TFSI	GAFF+0.70*RESP	298K 1bar	128	-	100	1
DEME-TFSI	GAFF+0.60*RESP	298K 1bar	128	-	100	1
DEME-TFSI	GAFF+0.55*RESP	298K 1bar	128	-	100	1
DEME-TFSI	GAFF+0.50*RESP	298K 1bar	128	-	100	1
DEME-TFSI	LJ pilot runs	298K 1bar	128	-	25	1
DEME-TFSI	refinedFF	298K 1bar	128	-	100	10
DEME-TFSI	refinedFF	313K 1bar	128	-	100	10
DEME-TFSI	refinedFF	333K 1bar	128	-	100	10
DEME-TFSI	refinedFF	353K 1bar	128	-	100	9
$N_{112,2O2O1}$-TFSI	refinedFF	298K 1bar	128	-	100	9
$N_{112,2O2O1}$-TFSI	refinedFF	313K 1bar	128	-	100	9
$N_{112,2O2O1}$-TFSI	refinedFF	333K 1bar	128	-	100	9
$N_{112,2O2O1}$-TFSI	refinedFF	353K 1bar	128	-	100	9

Table S3: Simulation run details used to estimate Ionic Conductivity, Shear Viscosity and X-ray Structure Factor.

Physical property	IL system	Force Field	State point	Ion Pairs	NPT (ns)	NVT (ns)	Independent runs
Ionic Conductivity	DEME-TFSI	refinedFF	298K 1bar	128	-	100	10
	DEME-TFSI	refinedFF	313K 1bar	128	-	100	10
	DEME-TFSI	refinedFF	333K 1bar	128	-	100	10
	DEME-TFSI	refinedFF	353K 1bar	128	-	100	9
	$N_{112,2O2O1}$-TFSI	refinedFF	298K 1bar	128	-	100	9
	$N_{112,2O2O1}$-TFSI	refinedFF	313K 1bar	128	-	100	9
	$N_{112,2O2O1}$-TFSI	refinedFF	333K 1bar	128	-	100	9
	$N_{112,2O2O1}$-TFSI	refinedFF	353K 1bar	128	-	100	9
Shear Viscosity	DEME-TFSI	refinedFF	298K 1bar	128	-	10	50
	DEME-TFSI	refinedFF	313K 1bar	128	-	10	50
	DEME-TFSI	refinedFF	333K 1bar	128	-	10	50
	DEME-TFSI	refinedFF	353K 1bar	128	-	10	30
	$N_{112,2O2O1}$-TFSI	refinedFF	298K 1bar	128	-	10	50
	$N_{112,2O2O1}$-TFSI	refinedFF	313K 1bar	128	-	10	50
	$N_{112,2O2O1}$-TFSI	refinedFF	333K 1bar	128	-	10	50
	$N_{112,2O2O1}$-TFSI	refinedFF	353K 1bar	128	-	10	30
X-ray Structure	DEME-TFSI	GAFF+0.60*RESP	298K 1bar	2056	30	30	1
	DEME-TFSI	GAFF+0.55*RESP	298K 1bar	2056	30	30	1
	DEME-TFSI	refinedFF	298K 1bar	2056	30	30	1
	$N_{112,2O2O1}$-TFSI	refinedFF	298K 1bar	2056	30	30	1

S4 Atomic Site Charges

S4.1 Classical MD simulations

Classical MD simulations of DEME-TFSI system containing eight ion pairs packed in a cubic box with periodic boundary conditions were carried out to obtain liquid phase snapshots for the subsequent condensed phase DFT calculations. The ions were packed in a cubic box using Packmol software. First, an energy minimization was carried out followed by 20 ns run performed in the isobaric-isothermal (NPT) ensemble. Subsequently, an isochoric-isothermal (NVT) simulation was run for 50 ns at the converged density ($\approx$ 16Å box size) obtained from the NPT simulation. Eight snapshots were extracted from the last 40 ns trajectory each separated by 5 ns. MD simulations were run with GAFF force field and RESP charges calculated from the isolated ion calculations at HF/6-31g(d) level. All other details are the same as for the bulk MD simulations mentioned in the main text.

S4.2 Condensed phase DDEC/c6 charges

The charges obtained from the condensed phase calculations are symmetrized according to the atom types. The net charges of the terminal methyl groups of the two ethyl groups of the cation are set to zero to allow for better transferability. The residual charge was redistributed over the rest of the atoms in a weighted manner, such that the highly charged groups get more of the residual charge.

The atomic site charges of DEME-TFSI system used in the refinedFF are listed in Table S4. The net ion charge of the DEME-TFSI and $N_{112,2O2O1}$-TFSI systems in the refinedFF are 0.8024 and 0.7640 respectively.

Table S4: Atomic site charges of the refined force field (refinedFF) of DEME-TFSI system. The net ion charge of this system is 0.8024. The nomenclature of atoms of DEME cation is shown in Figure S1

Atom Name	DDEC/c6[2,3] refinedFF
Cation Atomic Site Charges (e)	
N1	0.2223
C1/3	-0.0546
C2/4	-0.3900
C5	-0.3520
C6	-0.1545
C7	-0.0109
C8	-0.2796
H1/2/6/7	0.1126
H3/4/5/8/9/10	0.1300
H11/12/13	0.1612
H14/15	0.1309
H16/17	0.0691
H18/19/20	0.1356
O1	-0.2545
Anion Atomic Site Charges (e)	
N	-0.6474
S	0.9508
O	-0.5123
C	0.5228
F	-0.1755

Table S5: Atomic site charges of the refined force field of $N_{112,2O2O1}$-TFSI system. The net ion charge of this system is 0.7640. The nomenclature of atoms of $N_{112,2O2O1}$ cation is shown in Figure S4

Atom Name	DDEC/c6[2,3] refinedFF
Cation Atomic Site Charges (e)	
N1	0.2222
C1/2	-0.3520
C3	-0.0546
C4	-0.3900
C5	-0.1545
C6/7/8	-0.0109
C9	-0.2796
H1-H6	0.1612
H7-H8	0.1129
H9-H11	0.1300
H12-H13	0.1309
H14-H19	0.0691
H20-H22	0.1356
O1/2	-0.2545
Anion Atomic Site Charges (e)	
N	-0.6164
S	0.9053
O	-0.4878
C	0.4978
F	-0.1671

S5 QM-PES

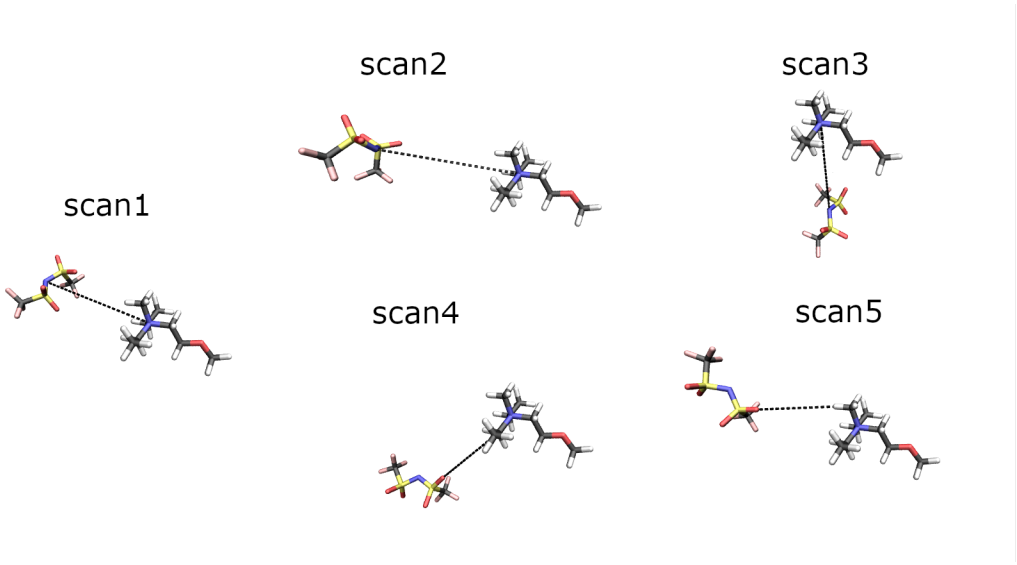

Figure S8: Molecular representations of the ion pair distance scan directions used to create the QM-PES.

Nine ion pair distance scans were constructed using Gaussview software out of which five scans were selected for QMC procedure. The five selected scan directions are shown as black dashed lines in the Figure S8.

S6 Quenched Monte Carlo

The QMC algorithm can be understood in three major steps, as follows:

- **Move:** A random perturbation (δ) is introduced to the current parameter set (ρ_{curr}) to generate a new guess parameter set ρ_{guess} (see equation S2). The size of the perturbation, referred to as the step size, depends on the user-defined input called the sensitivity (ρ_{sens}). The sensitivity setting allows the user to control how finely a particular atom type LJ parameter needs to be tuned. The loss function associated with ρ_{guess} is then calculated.

$$\rho_{guess} = \rho_{curr} + \delta * \rho_{sens} \tag{S2}$$

- **Metropolis Criteria:** The guess parameter ρ_{guess} is accepted as the next parameter ρ_{new} with a probability P_{acc} as shown in equation S4. All moves that decrease the loss function are accepted and moves that increase the loss function are accepted with the probability $e^{-\beta * \Delta L}$. This particular feature of the QMC allows for the parameters to escape the trap of local minima by climbing over barriers. Here β plays the role of inverse temperature. Low β values lead to high acceptance probability and inturn allowing the exploration of the parameter space. QMC makes use of this feature, by starting with a low β value allowing the parameters to move out of local minima. Once that is done, by gradually increasing the β value, the parameters are made to settle into a likely global minima. The details of this β scheduling is given in a later section.

$$\Delta L = L(\rho_{guess}) - L(\rho_{curr}) \tag{S3}$$

$$P_{acc} = min(e^{-\beta * \Delta L}, 1) \tag{S4}$$

- **Convergence Criteria:** Finally, a set of convergence criteria are used to check if the parameters have reached sufficiently close to the minima. In this case, we use the number of Monte Carlo iterations as the convergence criterion. If the final parameters are not satisfactory, then the Monte Carlo procedure is restarted with the final parameter as the initial guess.

The QMC algorithm in its generic form rarely yields the optimum result and needs to be tuned to the particular system at hand.[4,5] The following features were added to modify QMC into a bespoke tool to optimize the LJ parameters of ionic liquid systems.

- **quenching schedule:** We divide the Monte Carlo iterations into two logical parts. In the first run, called the equilibration run, β is started with a low value and gradually increased. This allows the parameters to explore the space and possibly get rid of the dependence on the initial guess. From the equilibration run, the best parameter set (need not be the last parameter set) is chosen as the initial guess for the subsequent run. In the next run, called the production run, the β value is set to a relatively high value to let the parameter set to settle near a global minima. Suitable values for the quenching rate of the production run depends on the system details like - the number of scan directions, weights in the calculation of RMSE, number of Monte Carlo steps etc. and reasonable values for this system were arrived at through experimentation.

  As a consequence of increasing the β value, the acceptance ratio (ratio of the number of accepted moves to the total number of moves) decreases. This will result in a wastage of computational resources as the rejected moves do not contribute to the final objective. This issue is tackled by tuning the sensitivity as explained in the following sections.

- **Bounds and sensitivity:** Bounds on the parameter set are necessary to ensure that the parameters remain physically meaningful. In the case of LJ parameters, both sigma and epsilon values must be positive and should be close to the generally accepted values as reported in general force fields. Also, choosing bounds carefully can ensure that the

parameter values are consistent with our chemical intuition. For example, we expect that the sigma of hydrogen atoms to be smaller than that of heavy atoms like carbon, nitrogen and oxygen. Sensitivity setting allows the user to adjust the magnitude of the perturbation in each Monte Carlo step. This is particularly useful if one intends to tune different species at different accuracy. For example, hydrogen atoms are particularly sensitive to their environment when compared to heavy atoms like nitrogen and carbon. For this reason, GAFF has five hydrogen atom types as opposed to one sp3 carbon atom type. Hence it is reasonable to tune hydrogens and heavy atoms at different accuracy. The bounds and sensitivity values of the LJ parameters used in this work are shown in table S6.

Table S6: Bounds and sensitivity (ρ_{sens}) of the LJ parameters used in the QMC procedure.

Atom types	σ(Å)			ϵ(kJ/mol)		
	min	max	sens	min	max	sens
can4	3.20	5.00	0.2	0.01	2.0	0.02
cac3	3.40	4.00	0.2	0.01	2.0	0.02
cacn	3.40	5.00	0.2	0.01	2.0	0.02
cahx	1.00	2.00	0.2	0.01	2.0	0.02
cahc	1.00	2.00	0.2	0.01	2.0	0.02
cah1	1.00	2.10	0.2	0.01	2.0	0.02
caos	2.00	3.00	0.2	0.01	2.0	0.02
anc3	3.20	3.80	0.2	0.01	2.0	0.02
ans6	3.40	4.00	0.2	0.01	2.0	0.02
anne	3.00	3.50	0.2	0.01	2.0	0.02
ansy	3.40	4.00	0.2	0.01	2.0	0.02
anoo	2.50	3.50	0.2	0.01	2.0	0.02
anff	2.80	4.00	0.2	0.01	2.0	0.02

- **Controlling the acceptance ratio:** As the β is increased during the production run, the acceptance ratio decreases unless we decrease the move size as well. The acceptance ratio controller adjusts the move size so as to keep the acceptance ratio at a preset constant value. A Proportional-Integral-Derivative (PID) control mechanism is used to keep tight control over the acceptance ratio.

S6.1 Loss function and configuration weights

$$L(\rho) = \sqrt{\sum_{\kappa} W_{\kappa} \left[E_{FF}(\rho;\kappa) - E_{QM}(\kappa)\right]^2} \tag{S5}$$

The loss function $L(\rho)$ for each scan direction is calculated independently using equation S5 and its average over the scans gives the total loss function used in the QMC procedure (equation S6). Here κ are the configurations of the PES, W_{κ} are the corresponding weights. The weight factors W_{κ} are additional user-defined parameters that can be used to relatively scale the error between $\mathrm{E}_{FF}(\rho;\kappa)$ and $\mathrm{E}_{QM}(\kappa)$ across different configurations. In the current context of fitting FF-PES to QM-PES, we assign higher weight values to configurations of lower energies (more stable configurations). This directs the optimizer to prioritize the fitting of low energy configurations. It is possible to assign the weights based on a predefined function of QM energy, which will be explored in future studies. Tables S7-S11 show the unnormalized weights for configurations in used all five scans. The normalization is done for each scan independently by dividing each of the unnormalized weights by the corresponding sum over all configurations in that particular scan.

$$L_{tot}(\rho) = (2 * L_1(\rho) + L_2(\rho) + L_3(\rho) + L_4(\rho) + L_5(\rho))/6 \tag{S6}$$

The loss function of scan1 was consistently higher than that of all other scans and hence its loss function contribution to the total was doubled as shown in equation S6. Here L_{tot} is the total loss used by the QMC and L_i corresponds to the loss function of scan i.

Table S7: Unnormalized weights used in scan 1.

Scan distance (Å)	Energy (kJ/mol)	W_κ
3.70	2.3	0.0
3.90	-140.8	100.0
4.10	-217.1	100.0
4.30	-253.1	1000.0
4.50	-265.1	10000.0
4.70	-263.0	10000.0
4.90	-253.7	1000.0
5.10	-240.6	1000.0
5.30	-226.4	1000.0
5.50	-212.5	100.0
5.70	-199.9	1.0
5.90	-188.7	1.0
6.10	-178.5	1.0
6.50	-161.0	1.0
7.00	-142.2	1.0
10.00	-73.9	1.0
14.00	-31.2	1.0
20.00	0.0	1.0

Table S8: Unnormalized weights used in scan 2.

Scan distance (Å)	Energy (kJ/mol)	W_κ
2.7	160.2	0.0
2.9	-53.6	0.0
3.1	-176.0	100.0
3.3	-238.7	1000.0
3.5	-264.2	10000.0
3.7	-267.9	10000.0
3.9	-260.2	10000.0
4.1	-247.5	1000.0
4.3	-232.6	1000.0
4.5	-218.2	100.0
4.7	-205.6	10.0
4.9	-193.0	10.0
5.1	-182.8	10.0
5.3	-173.0	1.0
5.5	-164.3	1.0
5.7	-156.1	1.0
5.9	-148.5	1.0
6.1	-141.5	1.0
6.3	-134.8	1.0
7.0	-115.0	1.0
10.0	-62.6	1.0
14.0	-27.0	1.0
20.0	0.0	1.0

Table S9: Unnormalized weights used in scan 3.

Scan distance (Å)	Energy (kJ/mol)	W_κ
3.3	-129.1	0.0
3.5	-218.7	0.0
3.7	-260.8	1000.0
3.9	-274.5	10000.0
4.1	-271.6	10000.0
4.3	-260.2	1000.0
4.5	-245.7	1000.0
4.7	-230.3	1000.0
4.9	-215.6	1000.0
5.1	-202.5	100.0
5.3	-190.7	100.0
5.5	-180.8	100.0
5.7	-171.5	100.0
5.9	-163.0	100.0
6.1	-155.1	100.0
6.3	-147.7	10.0
7.0	-125.5	1.0
10.0	-67.5	1.0
14.0	-29.0	1.0
20.0	0.0	1.0

Table S10: Unnormalized weights used in scan 4.

Scan distance (Å)	Energy (kJ/mol)	W_κ
2.30	-144.2	0.0
2.40	-163.9	0.0
2.50	-175.9	0.0
2.55	-180.1	10.0
2.60	-182.9	100.0
2.65	-184.9	1000.0
2.70	-186.1	10000.0
2.75	-186.7	10000.0
2.80	-186.7	10000.0
2.85	-186.3	10000.0
2.90	-185.5	1000.0
3.00	-183.0	100.0
3.50	-164.1	100.0
4.00	-145.2	100.0
5.00	-116.6	10.0
6.00	-94.5	10.0
8.00	-64.9	10.0
10.0	-45.2	1.0
12.0	-31.9	1.0
14.0	-21.0	1.0
15.0	-16.5	1.0
20.0	0.0	1.0

Table S11: Unnormalized weights used in scan 5.

Scan distance (Å)	Energy (kJ/mol)	W_κ
1.00	118.6	0.0
1.50	-166.2	1.0
1.70	-187.2	10.0
1.80	-190.3	1000.0
1.85	-190.8	10000.0
1.90	-190.7	10000.0
1.95	-190.1	10000.0
2.00	-188.9	1000.0
2.10	-185.7	1000.0
2.30	-177.5	100.0
2.40	-173.0	100.0
2.50	-168.4	10.0
2.55	-166.7	10.0
2.60	-163.9	1.0
2.70	-159.6	1.0
2.80	-155.6	1.0
3.00	-147.9	1.0
4.00	-117.5	1.0
6.00	-79.6	1.0
8.00	-56.2	1.0
10.00	-39.8	1.0
15.00	-14.8	1.0
20.00	0.0	1.0

S6.2 LJ pilot run details

Table S12: Performance of LJ pilot runs. Diffusion coefficient values are given in 10^{-11} m^2/s units.

LJ set (ρ)	run type	$L(\rho)$ kJ/mol	density kg/m^3	error (%)	D_+	error (%)	D_-	error (%)
GAFF	-	30.16	1445.9	2.77	0.07	-96.51	0.05	-96.85
refinedFF	-	24.60	1399.0	-0.55	1.69	-2.00	1.54	0.90
qmcff1	run2	12.03	1444.4	2.66	1.98	-1.49	2.10	20.00
qmcff2	run1	12.44	1468.4	4.37	2.10	4.48	1.70	-2.86
set1	run1	10.15	1218.2	-13.41	-	-	-	-
set2	run1	11.12	1367.5	-2.80	10.73	433.83	8.05	360.00
set3	run2	11.57	1430.3	1.67	2.94	46.27	3.09	76.57
set4	run2	11.59	1426.1	1.35	2.84	35.24	2.47	41.14
set5	run1	12.14	1431.4	1.74	3.22	60.20	2.50	42.29

Table S13: LJ parameters of the parameters sets selected for the pilot simulations. σ is in Åunits and ϵ is in kJ/mol units.

Atom types	qmcff2		set1		set2		set3		set4		set5	
	σ	ϵ	σ	ϵ	σ	ϵ	σ	ϵ	σ	ϵ	σ	ϵ
can4	5.000	0.5855	4.997	0.6103	4.999	0.6118	4.998	0.4392	4.994	0.4370	5.000	0.5987
cac3	3.421	0.1908	4.015	0.0117	3.601	0.0624	3.402	0.7344	3.401	0.7356	3.427	0.1635
cacn	3.421	0.1908	4.015	0.0117	3.601	0.0624	4.132	0.0101	4.141	0.0101	3.427	0.1635
cahx	1.997	0.0102	1.922	0.0101	1.984	0.0104	1.767	0.0110	1.779	0.0100	1.999	0.0107
cahc	1.321	0.0286	1.374	0.0191	1.239	0.0127	1.017	0.0105	1.031	0.0101	1.286	0.0104
cah1	1.621	0.0184	1.515	0.0682	1.670	0.0513	1.583	0.0317	1.614	0.0313	1.529	0.0454
caos	2.731	0.4762	2.751	0.4943	2.600	0.4760	2.641	0.6152	2.651	0.6138	2.746	0.4701
anc3	3.421	0.1908	4.015	0.0117	3.601	0.0624	3.237	0.7157	3.262	0.7140	3.427	0.1635
ans6	3.234	0.5225	3.213	0.5349	3.221	0.5594	3.481	0.3707	3.481	0.3685	3.336	0.5351
anne	2.974	0.3583	2.908	0.3831	2.905	0.3723	3.001	0.7031	3.016	0.7005	2.961	0.3546
ansy	3.232	0.4511	3.266	0.4510	3.477	0.4381	3.411	0.8553	3.406	0.8558	3.245	0.4575
anoo	3.399	0.9582	3.398	0.9866	3.394	0.9678	3.478	0.9909	3.487	0.9930	3.399	0.9743
anff	2.812	0.2823	3.152	0.2125	2.897	0.2184	3.118	0.0314	3.132	0.0292	2.947	0.2481

S7 Results

The root mean squared (RMSE) of a simulated quantity with respect to the corresponding experimental value is defined as

$$RMSE = \sqrt{1/s \sum_{i}^{s} \left(X_{sim}^{i} - X_{exp}^{i}\right)^2} \tag{S7}$$

where s is the number of state points, X_{sim}^{i} and X_{exp}^{i} are the simulated and the corresponding experimental values at the state point i.

S7.1 Density

Table S14: Density of DEME-TFSI and $N_{112,2O2O1}$-TFSI liquids. The standard error on the mean of simulated density is less than the 1 kg/m^3. The simulation data is obtained using the refined force field and the experimental data is taken from refs[6–8]

System	Temperature (K)	Experimental (kg/m^3)	This work (kg/m^3)	Error (%)
DEME-TFSI	298	1407	1399	-0.55
	303	1402	1394	-0.58
	313	1392	1383	-0.70
	323	1384	1373	-0.83
	333	1375	1361	-1.03
	343	1366	1351	-1.14
	353	1357	1340	-1.30
$N_{112,2O2O1}$-TFSI	298	1391	1396	0.34
	303	1387	1390	0.27
	313	1377	1379	0.14
	323	1368	1368	-0.04
	333	1360	1357	-0.17
	343	1351	1346	-0.33
	353	1342	1335	-0.50

Table S15: Linear fit parameters of experimental (Exp) and simulated (Sim) density values. The error is in %. The simulation data is obtained using refined force field and the experimental data is taken from refs.[6–8]

System	Slope (kg/m^{3}K)			Intercept (kg/m^3)		
	Exp	Sim	Error	Exp	Sim	Error
DEME-TFSI	-0.8994	-1.0850	20.6	1675	1723	2.9
$N_{112,2O2O1}$-TFSI	-0.8969	-1.1040	23.1	1658	1725	4.0

S7.2 Liquid structure

To probe the mesoscopic ordering in the ionic liquids, coherent X-ray scattering intensity was calculated using,[9]

$$I_{coh}(q) = \sum_{\alpha} x_{\alpha} f_{\alpha}(q)^2 + \sum_{\alpha} \sum_{\beta} x_{\alpha} x_{\beta} f_{\alpha}(q) f_{\beta}(q) 4\pi\rho \int_0^{\infty} r^2 (g_{\alpha\beta}(r) - 1) \frac{sin(qr)}{qr} W(r) dr \quad \text{(S8)}$$

where $I_{coh}(q)$ is the wave-vector dependent coherent X-ray scattering intensity, x_{α} and x_{β} are the fractions of the atom types α and β respectively, $f_{\alpha}(q)$ is the X-ray atomic form factor of atom type α, ρ is the total atomic number density, $g_{\alpha\beta}(r)$ is the radial distribution function between species α and β, and $W(r)$ is the Lorch window function used to reduce the noise in $I(q)$ at low wave-vectors.[10] Simulations with large system size were used to calculate the X-ray scattering intensity in order to tease out any mesoscopic ordering. High temperature annealing was carried out to eliminate any ordering induced by the packing procedure. The system size details are given in Table S3.

The total and the partial X-ray structure factors are computed using the following relations.

$$S(q) = \frac{I_{coh}(q) - \sum_{\alpha} x_{\alpha} f_{\alpha}(q)^2}{\left(\sum_{\alpha} x_{\alpha} f_{\alpha}(q)\right)^2} \quad \text{(S9)}$$

$$S(q) = \frac{\sum_{\alpha} \sum_{\beta} x_{\alpha} x_{\beta} f_{\alpha}(q) f_{\beta}(q) 4\pi\rho \int_0^{\infty} r^2 (g_{\alpha\beta}(r) - 1) \frac{sin(qr)}{qr} W(r) dr}{\left(\sum_{\alpha} x_{\alpha} f_{\alpha}(q)\right)^2} \quad \text{(S10)}$$

$$S_{cation-cation}(q) = \frac{\sum_{\alpha}^{cation} \sum_{\beta}^{cation} x_{\alpha} x_{\beta} f_{\alpha}(q) f_{\beta}(q) 4\pi\rho \int_0^{\infty} r^2 (g_{\alpha\beta}(r) - 1) \frac{sin(qr)}{qr} W(r) dr}{\left(\sum_{\alpha} x_{\alpha} f_{\alpha}(q)\right)^2} \quad \text{(S11)}$$

$$S_{anion-anion}(q) = \frac{\sum_{\alpha}^{anion}\sum_{\beta}^{anion} x_\alpha x_\beta f_\alpha(q) f_\beta(q) 4\pi\rho \int_0^\infty r^2 (g_{\alpha\beta}(r)-1)\frac{sin(qr)}{qr} W(r) dr}{\left(\sum_\alpha x_\alpha f_\alpha(q)\right)^2} \quad \text{(S12)}$$

$$\begin{aligned} S_{cation-anion}(q) = & \frac{\sum_{\alpha}^{cation}\sum_{\beta}^{anion} x_\alpha x_\beta f_\alpha(q) f_\beta(q) 4\pi\rho \int_0^\infty r^2 (g_{\alpha\beta}(r)-1)\frac{sin(qr)}{qr} W(r) dr}{\left(\sum_\alpha x_\alpha f_\alpha(q)\right)^2} \\ & + \frac{\sum_{\alpha}^{anion}\sum_{\beta}^{cation} x_\alpha x_\beta f_\alpha(q) f_\beta(q) 4\pi\rho \int_0^\infty r^2 (g_{\alpha\beta}(r)-1)\frac{sin(qr)}{qr} W(r) dr}{\left(\sum_\alpha x_\alpha f_\alpha(q)\right)^2} \end{aligned} \quad \text{(S13)}$$

$$S(q) = S_{cation-cation}(q) + S_{anion-anion}(q) + S_{cation-anion}(q) \quad \text{(S14)}$$

where $I_{coh}(q)$ is the wave-vector dependent coherent X-ray scattering intensity, $S(q)$ is the total X-ray structure factor, $S_{cation-cation}(q)$ $S_{anion-anion}(q)$ and $S_{cation-anion}(q)$ are the partial structure factors corresponding to cation-cation anion-anion and cation-anion correlations respectively, x_α and x_β are the fractions of the atom types α and β respectively, $f_\alpha(q)$ is the X-ray atomic form factor, ρ is the total atomic number density, $g_{\alpha\beta}(r)$ is the radial distribution function between species α and β, and $W(r)$ is the Lorch window function used to reduce the noise in $S(q)$ at low wave-vectors.

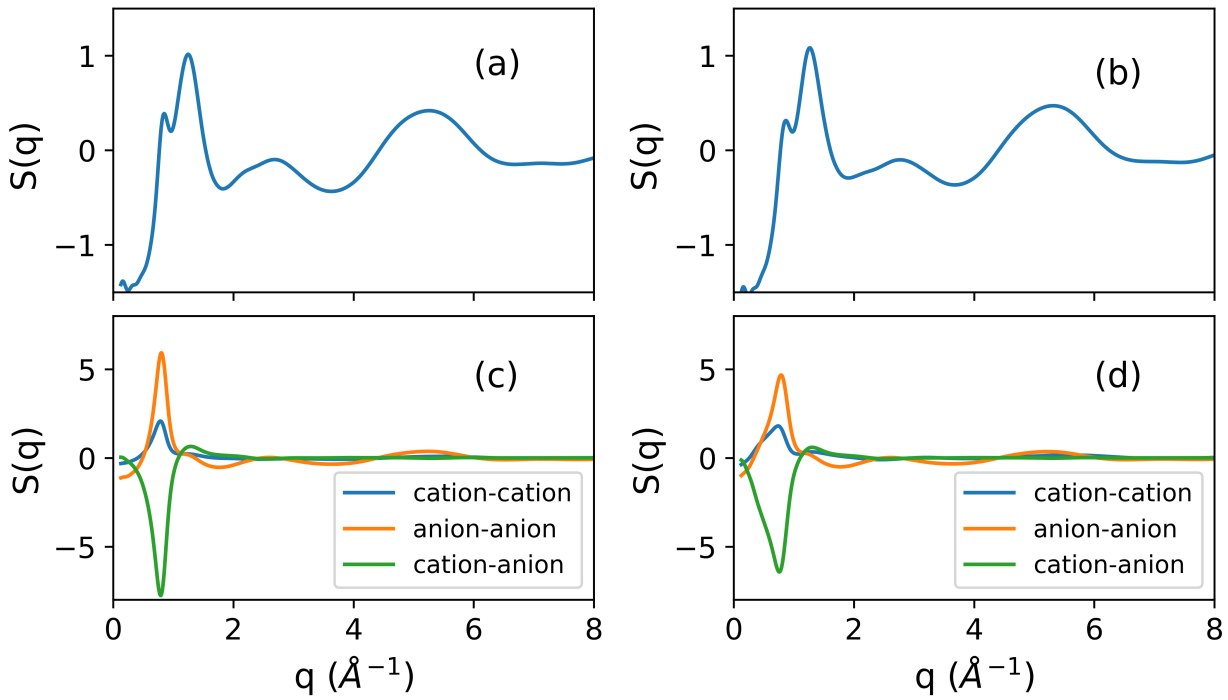

Figure S9: (a) and (c) show the total and partial X-ray structure factors of DEME-TFSI liquid respectively. (b) and (d) show the total and partial structure factors of $N_{112,2O2O1}$-TFSI system respectively. Both these systems were simulated using the refined force field at 298 K.

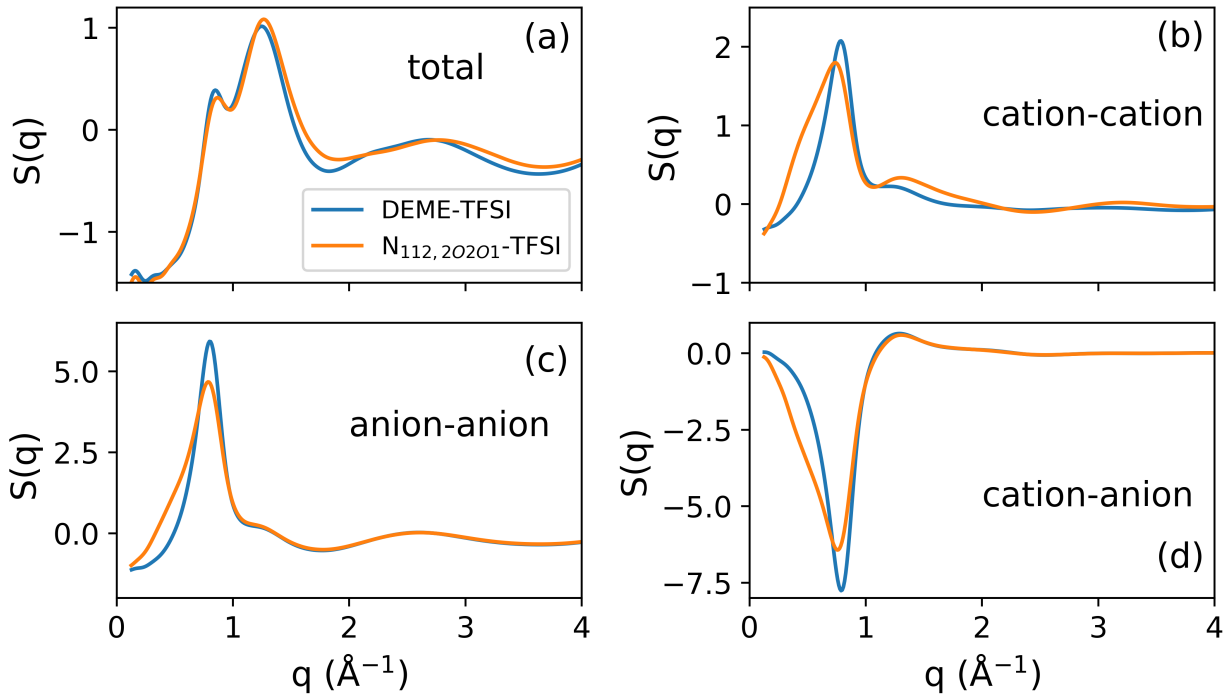

Figure S10: Comparison of the total and partial X-ray structure factors of DEME-TFSI system (blue line) and $N_{112,2O2O1}$-TFSI system (orange line). Both these systems were simulated using the refined force field at 298 K.

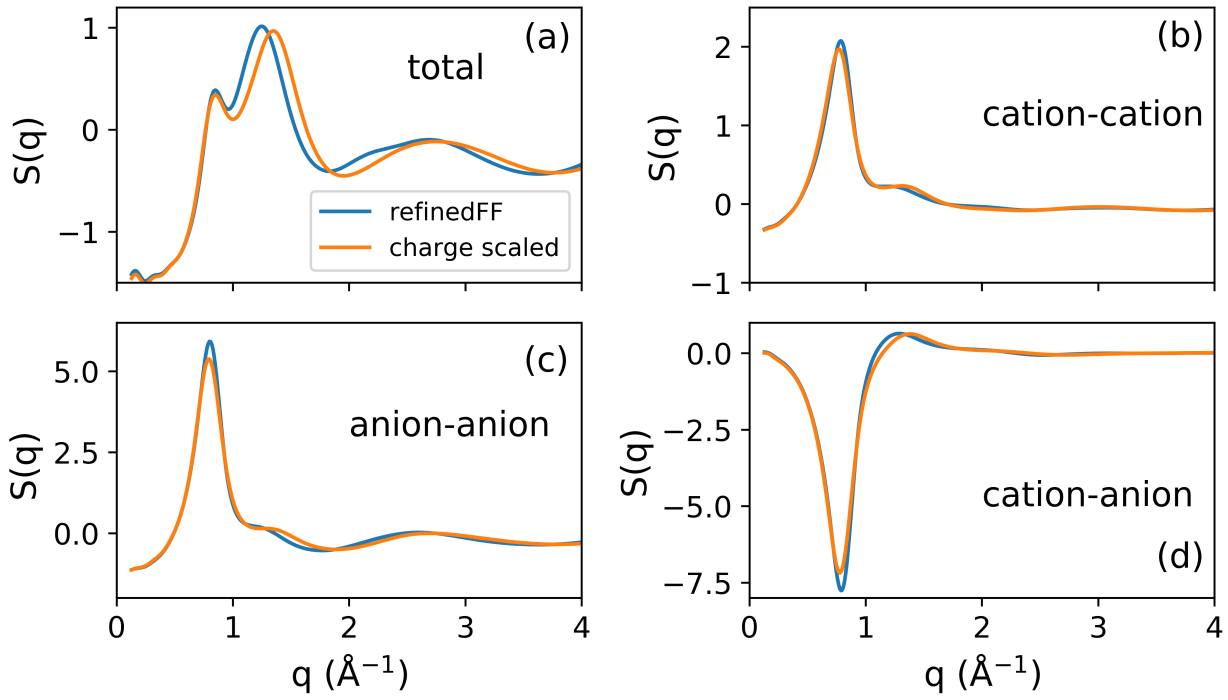

Figure S11: Comparison of the total (a) and partial (b-d) X-ray structure factors of DEME-TFSI system using refined force field (blue line) and uniform charge scaled (0.55 scaling factor) GAFF force field (orange line). Both the systems were simulated at 298 K.

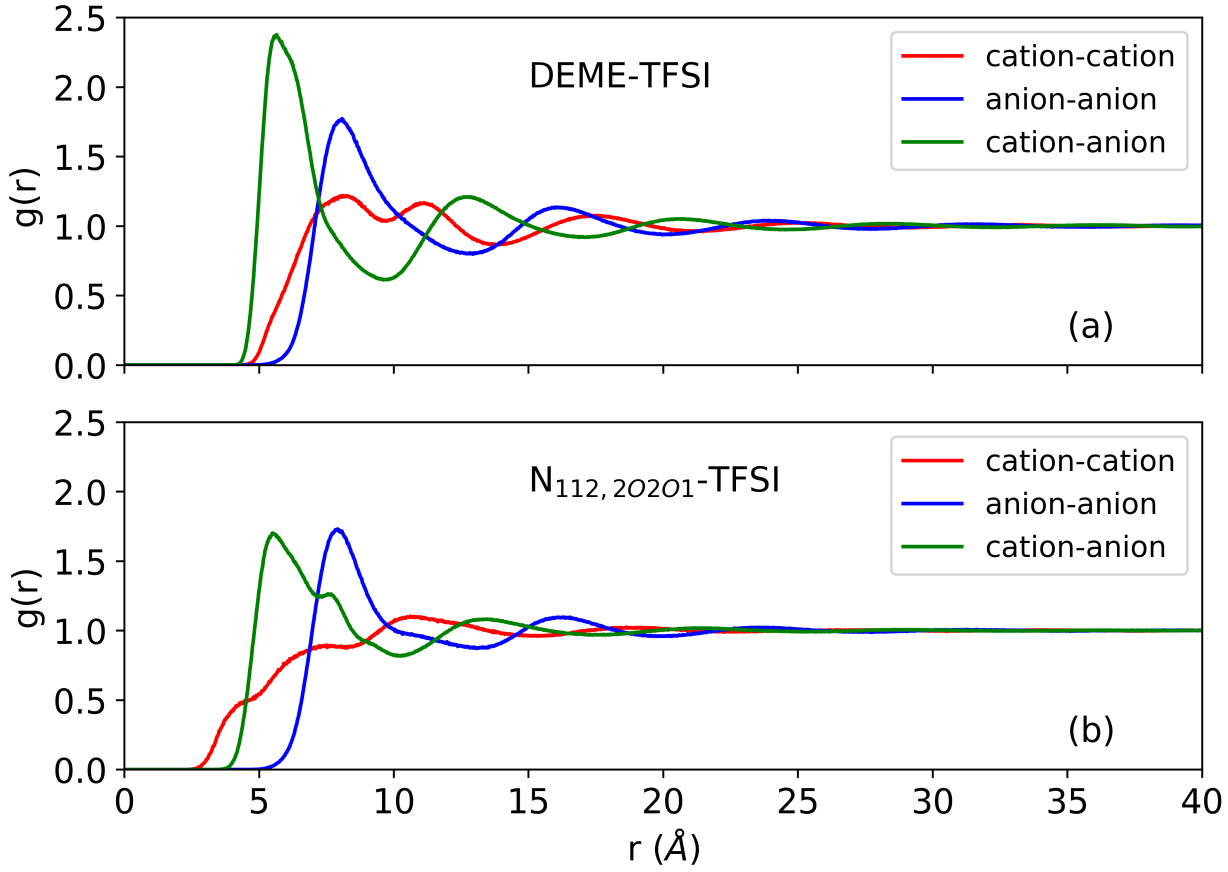

Figure S12: Radial distribution functions between the cation-cation, cation-anion and anion-anion center of masses of (a) DEME-TFSI system and (b) $N_{112,2O2O1}$ system.

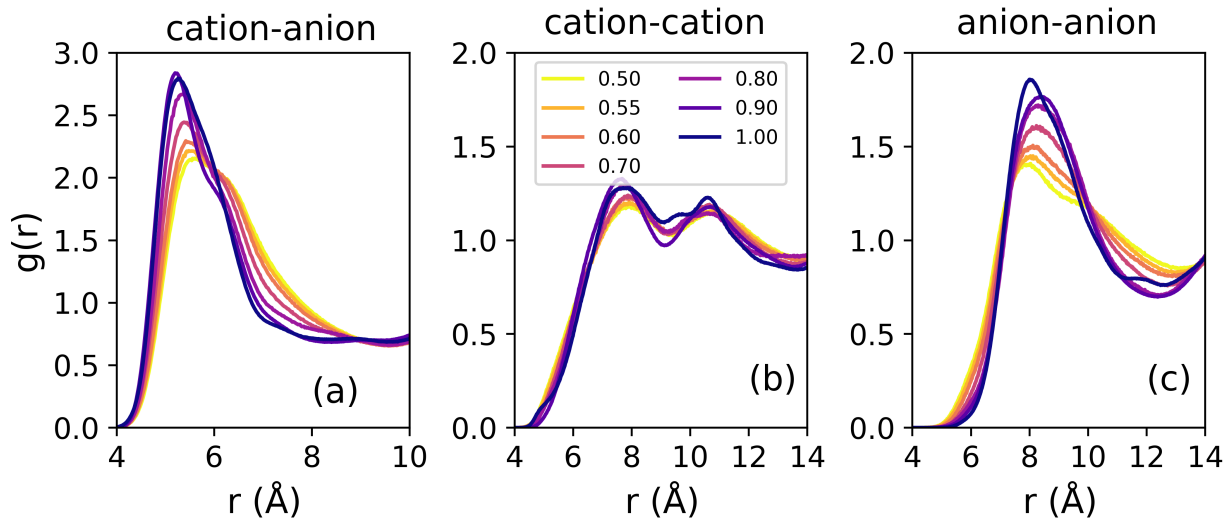

Figure S13: Radial distribution functions between the cation-cation, cation-anion and anion-anion center of masses at various uniform charge scaling factors. All the simulations were carried out with GAFF force field and charges were obtained by scaling the isolated ion RESP charges scaled by an uniform charge scaling factor. All the simulations were at 298 K.

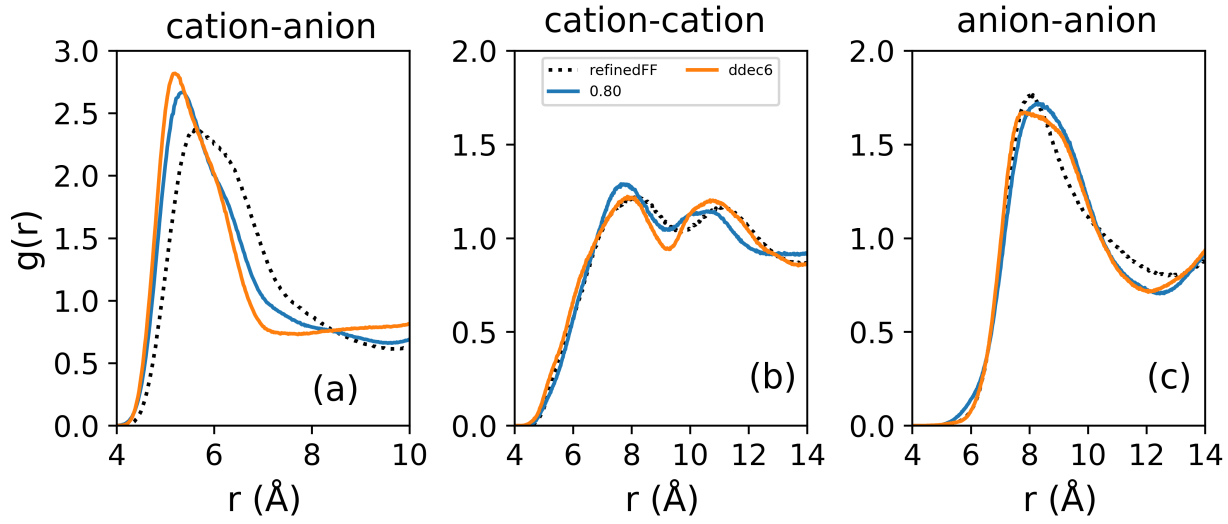

Figure S14: Comparison of radial distribution functions between the cation-cation, cation-anion and anion-anion center of masses with - refined force field (refinedFF as black dotted lines), GAFF force field with condensed phase DDEC/c6 charges (ddec6 as orange continuous lines), and GAFF force field with isolated ion RESP charges scaled by an uniform charge scaling factor of 0.80 (0.80 as blue continuous lines). All simulations were at 298 K.

S7.3 Self-Diffusion

The self-diffusion coefficients (D) of the ions were estimated from the corresponding center of mass (COM) mean squared displacements (MSD) using the Einstein relation (Eq S15).

$$D = \frac{1}{6} \lim_{t \to \infty} \frac{d}{dt} \left\langle \frac{1}{N} \sum_{i=1}^{N} (\boldsymbol{r}_i(t) - \boldsymbol{r}_i(0))^2 \right\rangle \tag{S15}$$

Here, N is the number of ions for which the diffusion coefficient is being calculated, $\boldsymbol{r}_i(t)$ is the position of the center of mass of the ion i at time t and $\langle\rangle$ denotes the averaging over time origins. The MSD of ionic liquids (and most dense liquids) shows a ballistic region (MSD $t^\beta, \beta = 2$) at short times followed by a plateau region (MSD $t^\beta, \beta < 1$) and then the diffusive region (MSD $t^\beta, \beta = 1$) at long times. In practice however, the long time behavior of the MSD is dominated by noise due to poor statistics and hence the "middle region" of the MSD is usually used to obtain the diffusion coefficients. The exponent $\beta(t)$ (Eq S16) can be used to unambiguously identify the diffusive region of the MSD.

$$\beta(t) = \frac{d(ln(MSD(t)))}{d(ln(t))} \tag{S16}$$

Here, ln() denotes the natural logarithm and MSD(t) is the mean squared displacement at time t. Figure S15 shows the behaviour of MSD and β vs time for the DEME-TFSI system at 298K. The log-log plot (Figure S15(b)) clearly shows the three regions of the MSD which are not directly evident from the linear plot (Figure S15(a)). Figures S15(c) and (d), show the behaviour of β vs time for cation and anion respectively. β reaches 1 at about 10 ns and continues to fluctuate around 1 till about 50 ns after which noise starts to dominate.

Table S16 and Figures S16, S17 show the time windows chosen to calculate the diffusion coefficients. These time windows were divided into five equal blocks to estimate the standard error on the mean using block averaging method.[11] The white circles in Figure S15 (c) and (d), show the β values in each of the five blocks. Figures S16 and S17 show the behaviour of

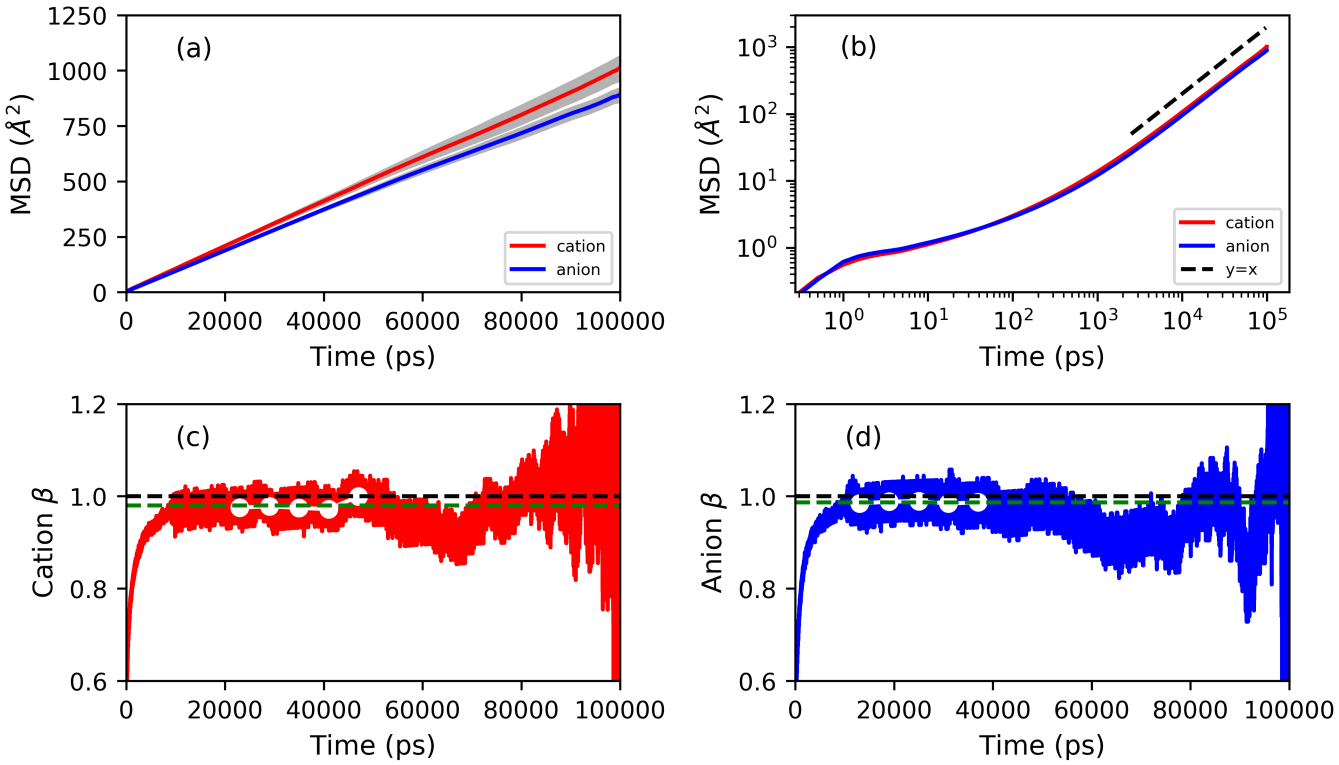

Figure S15: (a) MSD of DEME cations (red) and TFSI anions (blue) in DEME-TFSI ionic liquid at 298K. The grey shaded region around the dark lines indicate the standard error on the mean. (b) The same data plotted in log-log scale reveals the three regions of MSD. The black dashed line, with a unit slope, is drawn as a guide to the eye. (c) and (d) show the β vs time for the cations and anions respectively. The black horizontal dashed line indicates $\beta = 1$ and the green horizontal dashed line indicates the average β from the selected time window. The white circles indicate the average β values in each of the five blocks.

β vs time for DEME-TFSI and $N_{112,2O2O1}$-TFSI systems respectively at four temperatures.

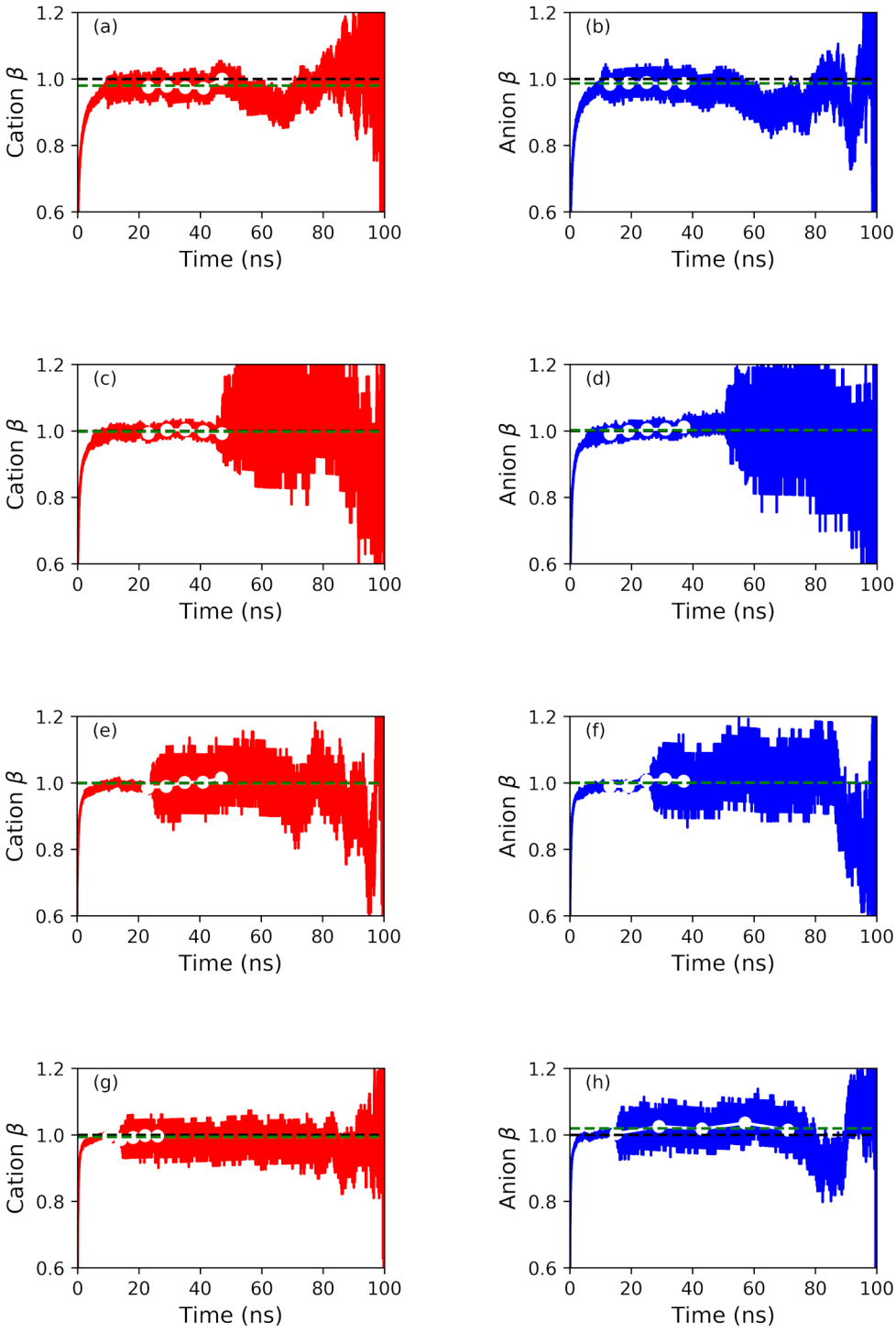

Figure S16: The time evolution of $\beta(t)$ of the DEME cation (a),(c),(e),(g) and the TFSI anion (b),(d),(f),(h) at 298 K, 313 K, 333 K and 353 K respectively.

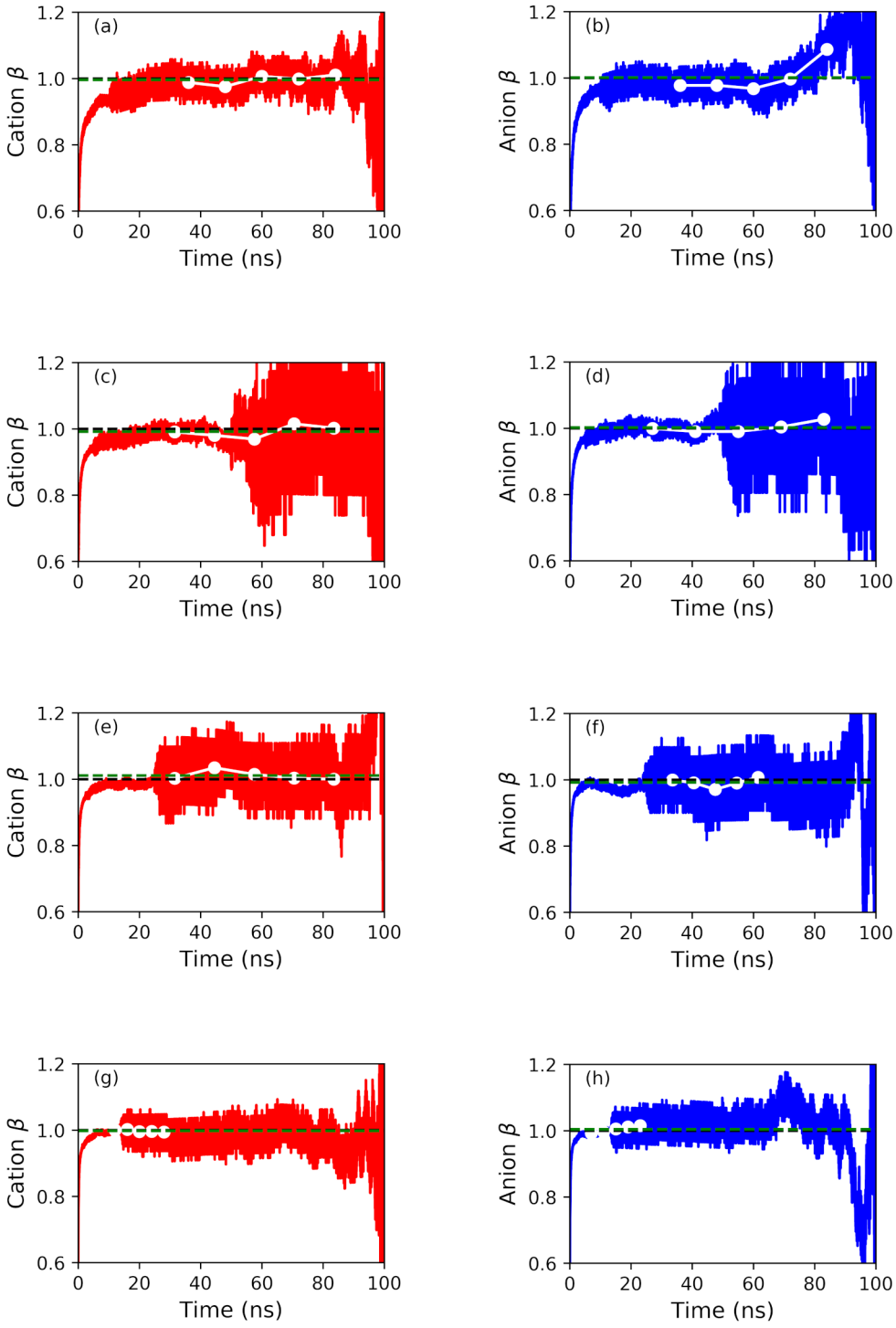

Figure S17: The time evolution of $\beta(t)$ of the $N_{112,2O2O1}$ cation (a),(c),(e),(g) and the TFSI anion (b),(d),(f),(h) at 298 K, 313 K, 333 K and 353 K respectively.

Table S16: Time windows used to fit a straight line to the MSD(t) and the corresponding average beta values.

System	Tempera-ture(K)	Cation			Anion		
		t_{start} (ns)	t_{end} (ns)	Average β	t_{start} (ns)	t_{end} (ns)	Average β
DEME-TFSI	298	20	50	0.980	10	40	0.987
	313	20	50	0.998	10	40	1.002
	333	20	50	0.999	10	40	1.001
	353	8	28	0.994	8	78	1.020
$N_{112,2O2O1}$-TFSI	298	30	90	0.996	30	90	1.001
	313	25	90	0.992	20	90	1.002
	333	25	90	1.011	30	65	0.992
	353	10	30	0.998	5	25	1.004

Table S17: Self-diffusion coefficient values of our refined force field model and their comparison to the respective experimental values.[6–8] The standard error on the mean of the diffusion coefficient values are less than $0.05 * 10^{-11} m^2/s$.

System	Tempera-ture(K)	Cation D (10^{-11} m^2/s)			Anion D (10^{-11} m^2/s)		
		Experimental	This work	Error (%)	Experimental	This work	Error (%)
DEME-TFSI	298	1.72	1.685	-2.0	1.53	1.544	0.9
	313	3.50	3.378	-3.5	3.11	3.052	-1.9
	333	6.95	6.601	-5.0	6.37	5.961	-6.4
	353	12.30	11.473	-6.7	11.70	10.984	-6.1
$N_{112,2O2O1}$-TFSI	298	1.82	1.489	-18.2	1.62	1.565	-3.3
	313	3.46	2.991	-13.6	3.27	3.231	-1.3
	333	6.74	6.553	-2.8	6.12	6.502	6.2
	353	11.72	11.649	-0.6	10.93	12.166	11.3

S7.3.1 Box size correction

The correction to the self-diffusion coefficient due to the finite simulation box size (with periodic boundary conditions) was given by Yeh and Hummer[12] as

$$D_{YH} = \frac{2.837298 k_B T}{6\pi\eta L} \tag{S17}$$

Where, D_{YH} is the correction term, k_B is the Boltzmann's constant, T is the absolute temperature, η is the calculated viscosity and L is the box size.

Table S18: Box size correction to the self-diffusion coefficient values using the Yeh-Hummer (YH) formula.[12] The correction term is in the units: $10^{-11} m^2/s$.

System	Tempera-ture(K)	Viscosity (mPa.s)	Box size (Å)	YH Correction term	Corrected D (10^{-11} m^2/s)	
					Cation	Anion
DEME-TFSI	298	54.9	40.1618	0.28	1.966	1.825
	313	29.9	40.3210	0.54	3.918	3.592
	333	15.1	40.5354	1.13	7.734	7.094
	353	8.9	40.7473	2.03	13.500	13.011
$N_{112,2O2O1}$-TFSI	298	61.8	41.1164	0.24	1.733	1.809
	313	29.2	41.2785	0.54	3.530	3.770
	333	14.6	41.5020	1.14	7.697	7.646
	353	8.7	41.7310	2.02	13.670	14.187

S7.3.2 Temperature dependence and activation energy

Both experimental and simulations data were fit to Arrhenius equation of the type,

$$D = D_0 exp(-E_D/RT) \tag{S18}$$

where D is the self-diffusion coefficient at temperature T, E_D is the activation energy, D_0 is the prefactor and R is the universal gas constant. Tables S19 and S20 list the fit parameters of DEME-TFSI and $N_{112,2O2O1}$-TFSI systems.

Table S19: Activation energies of the diffusion coefficient in DEME-TFSI and $N_{112,2O2O1}$-TFSI systems.

System	Cation E_D (kJ/mol)			Anion E_D (kJ/mol)		
	Experimental	This work	error(%)	Experimental	This work	error(%)
DEME-TFSI	31.11	30.34	-2.5	32.21	30.96	-3.9
$N_{112,2O2O1}$-TFSI	29.54	32.87	11.3	30.00	32.35	7.9

Table S20: Prefactor in the Arrhenius fit of the diffusion coefficient.

System	Cation D_0 (10^{-8} m^2/s)			Anion D_0 (10^{-8} m^2/s)		
	Experimental	This work	error(%)	Experimental	This work	error(%)
DEME-TFSI	509	366	-28.2	700	424	-39.5
$N_{112,2O2O1}$-TFSI	282	887	214.2	306	760	148.5

S7.3.3 Uniform Charge Scaling

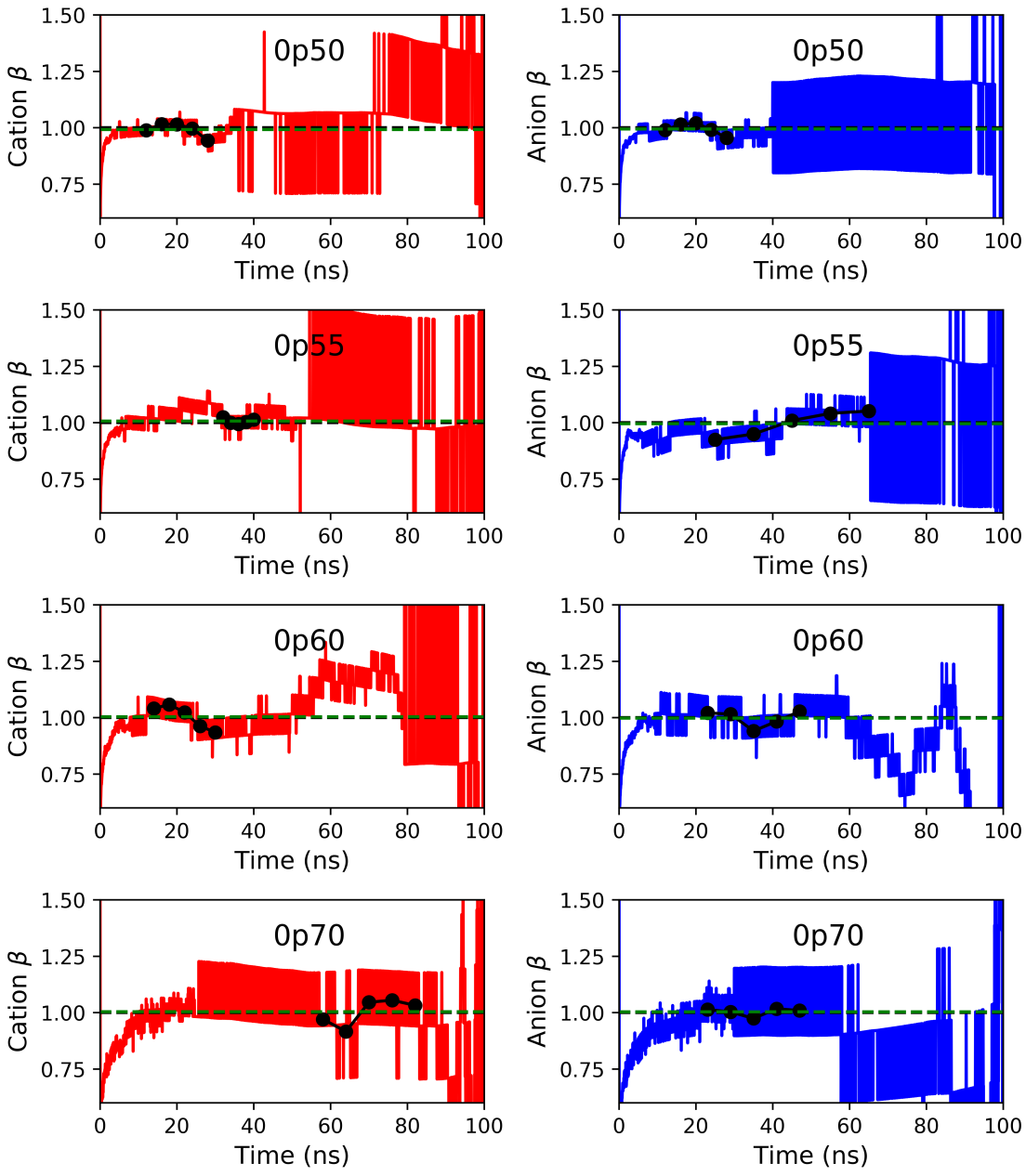

Figure S18: The time evolution of $\beta(t)$ of the DEME cation (red) and the TFSI anion (blue). The simulations were carried out with GAFF force field and isolated ion RESP charges scaled by an uniform charge scaling factor shown in the panels (XpYY should be read as X.YY). The black horizontal dashed line indicates $\beta = 1$ and the green horizontal dashed line indicates the average β from the selected time window. The black circles indicate the average β values in each of the five blocks.

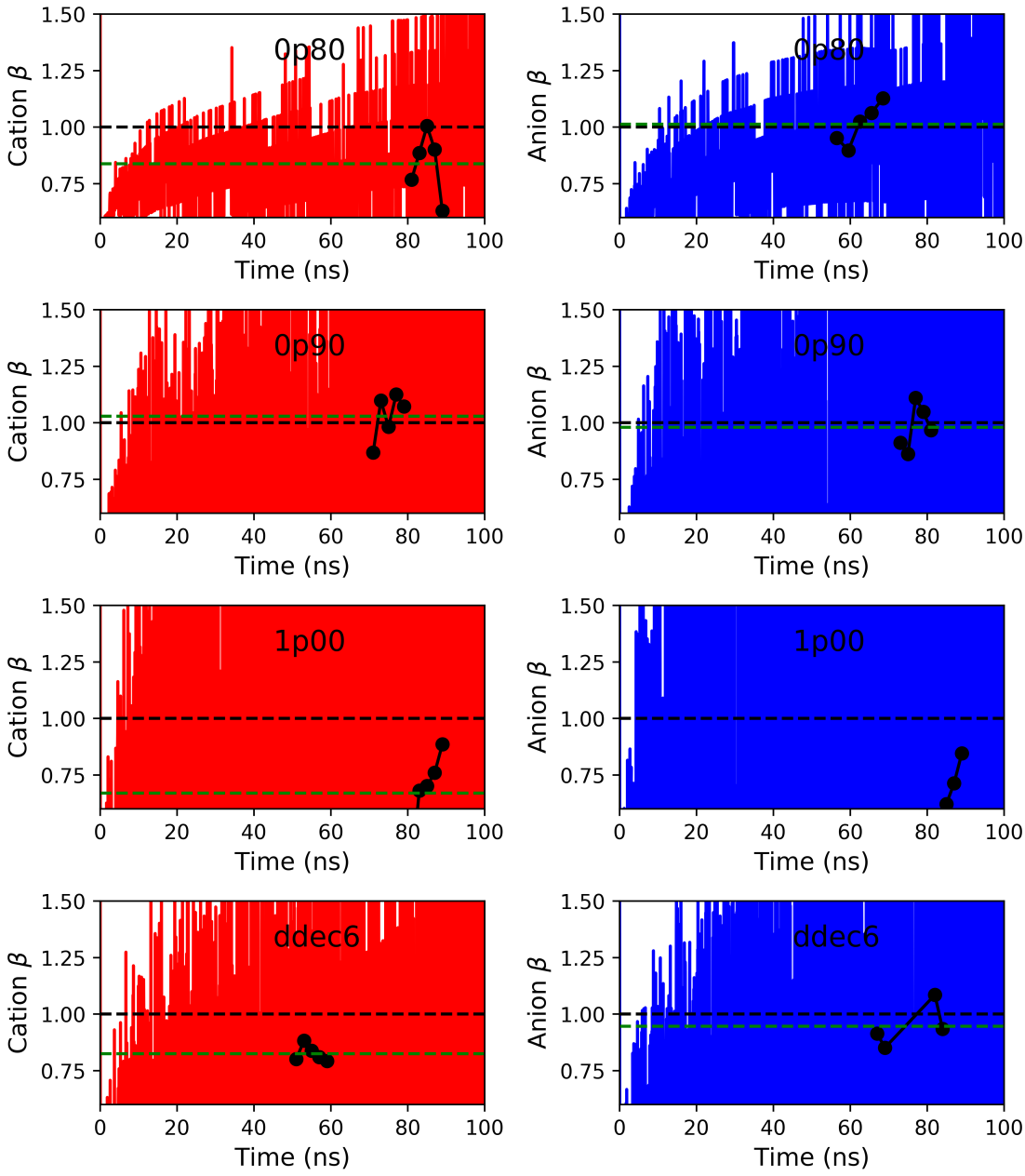

Figure S19: The time evolution of $\beta(t)$ of the DEME cation (red) and the TFSI anion (blue). The simulations were carried out with GAFF force field and isolated ion RESP charges scaled by an uniform charge scaling factor shown in the panels (XpYY should be read as X.YY). The black horizontal dashed line indicates $\beta = 1$ and the green horizontal dashed line indicates the average β from the selected time window. The black circles indicate the average β values in each of the five blocks.

S7.4 Ionic Conductivity

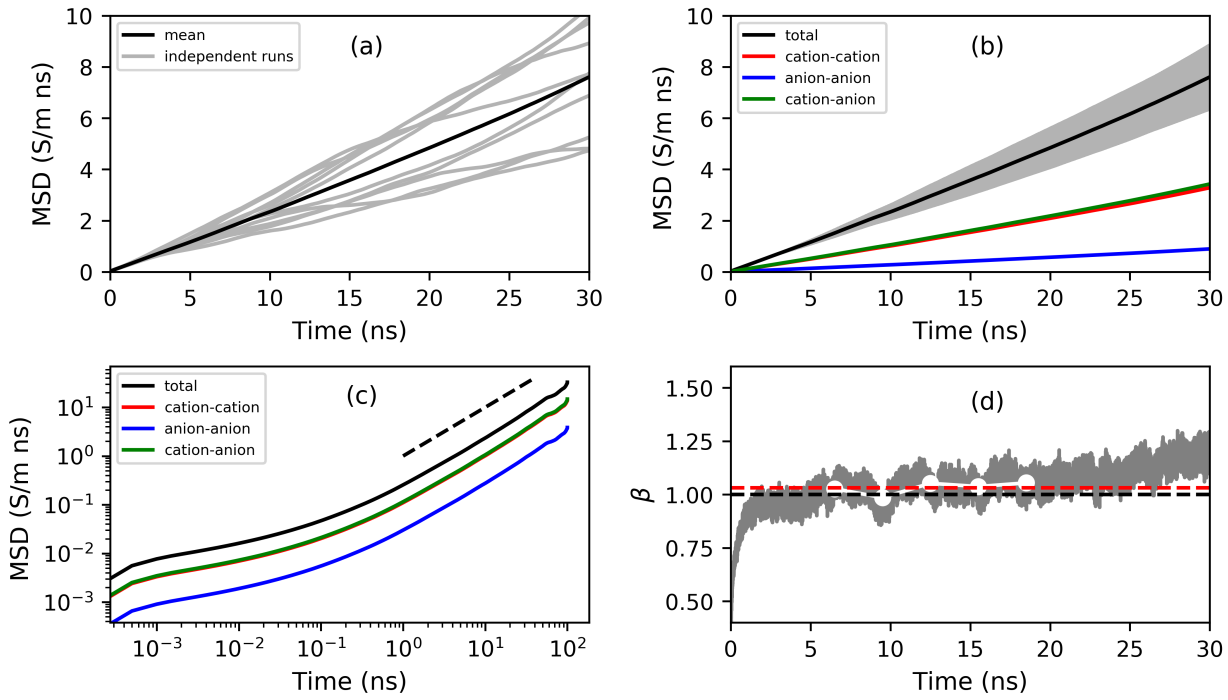

Figure S20: (a) The collective MSD of ten independent trajectories (grey) Averaging over multiple independent trajectories was necessary to get a smooth collective MSD (black). (b) The total and partial collective MSDs as a function of time. The grey shaded region around the black line is the standard error on the mean. (c) Collective MSDs in log-log scale reveal the "sub-diffusive" region. The black dashed line with a slope 1 is drawn as a guide to the eye. (d) β vs time was used to select the time window in which to fit the collective MSD. The black horizontal dashed line indicates $\beta = 1$ and the red horizontal dashed line is the average value of beta in the selected time window. The white circles show the β values in the five time blocks. All the data in this plot is from the DEME-TFSI system at 298 K.

The ionic conductivity was estimated using the Einstein relation,

$$\sigma = \frac{e^2}{6Vk_BT} \lim_{t\to\infty} \frac{d}{dt} \left\langle \sum_{i=1}^{N_{ion}} \sum_{j=1}^{N_{ion}} q_i\, q_j\, (\boldsymbol{r}_i(t) - \boldsymbol{r}_i(0)).(\boldsymbol{r}_j(t) - \boldsymbol{r}_j(0)) \right\rangle \tag{S19}$$

where e is the elementary charge, V is the volume of the simulation box, T is the temperature, k_B is the Boltzmann constant, N_{ion} is the total number of ions (both cations and anions), q_i and q_j are the net ion charges of the i^{th} and j^{th} ions respectively, $\boldsymbol{r}_i(t)$ is the position vector of center of mass of ion i at time t, and $\langle\rangle$ denotes the averaging over time

origins.

$$MSD(t) = \frac{e^2}{6Vk_BT} \left\langle \sum_{i=1}^{N_{ion}} \sum_{j=1}^{N_{ion}} q_i \, q_j \, (\boldsymbol{r}_i(t) - \boldsymbol{r}_i(0)).(\boldsymbol{r}_j(t) - \boldsymbol{r}_j(0)) \right\rangle \tag{S20}$$

At least nine independent NVT simulations of 100 ns each were run at each state point. For each independent simulation, the collective MSD (Equation S20) was calculated and were then averaged (Figure S20(a)). The long time slope of the collective MSD with respect to time yields the conductivity. Similar to the self-diffusion coefficient calculation, the long time behavior of the collective MSD is dominated by noise.[13] β(t) exponent (Eq S16) was used to identify the time windows from which the conductivity values were estimated as shown in Table S21 and Figures S21, S22. Each time window was further divided into five equal blocks and error analysis was done using the block averaging method.[11]

Table S21: Time windows used to fit a straight line to the collective MSD(t) and the corresponding average beta values.

System	Temperature (K)	t_{start} (ns)	t_{end} (ns)	Average β
DEME-TFSI	298	5	20	1.031
	313	5	20	1.007
	333	4	29	0.984
	353	2	17	1.016
$N_{112,2O2O1}$-TFSI	298	12	17	0.996
	313	15	25	0.993
	333	5	15	1.008
	353	3	13	1.007

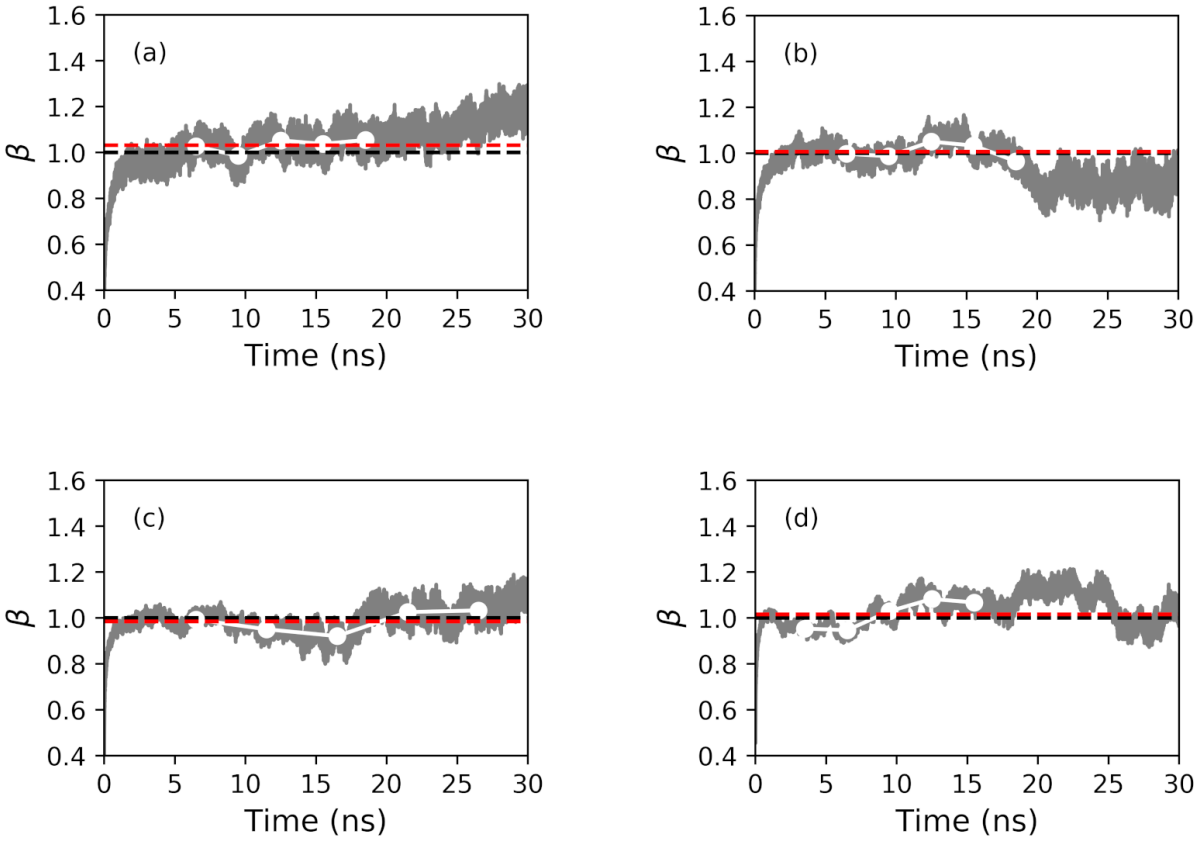

Figure S21: β (of the collective MSD) vs time of the DEME-TFSI system. (a),(b),(c),(d) correspond to 298 K, 313 K, 333 K and 353 K respectively. The black horizontal dashed line indicates $\beta = 1$ and the red horizontal dashed line is the average value of beta in the selected time window. The white circles show the β values in the five time blocks.

Table S22: Ionic conductivity values of our refined force field model and their comparison to the respective experimental values.[6–8] The standard error on the mean of the ionic conductivity are less than 0.03 S/m.

System	Temperature (K)	Ionic conductivity (S/m)		
		Experimental	This work	Error (%)
DEME-TFSI	298	0.260	0.244	-6.2
	313	0.488	0.412	-15.6
	333	0.869	0.665	-23.5
	353	1.330	1.169	-12.1
$N_{112,2O2O1}$-TFSI	298	0.257	0.171	-33.5
	313	0.451	0.324	-28.2
	333	0.809	0.619	-23.5
	353	1.269	1.021	-19.4

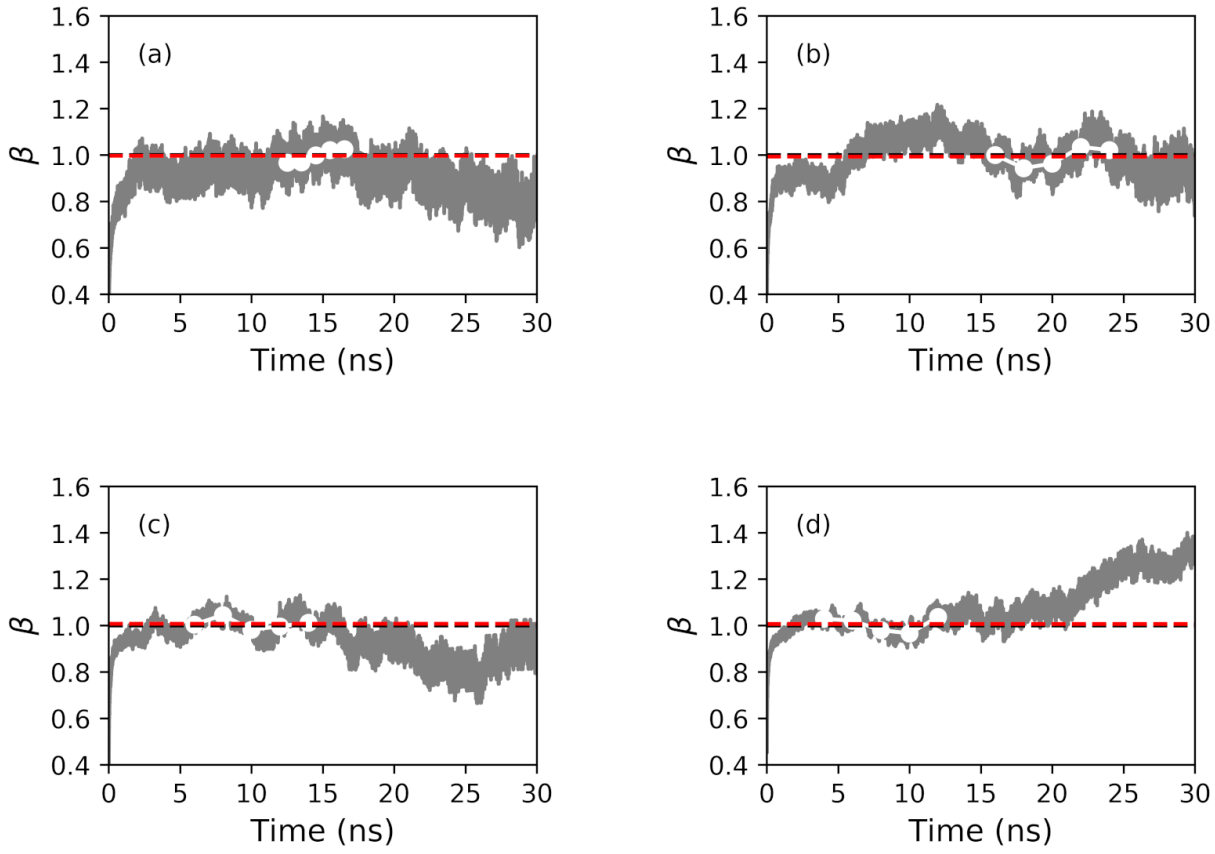

Figure S22: β (of the collective MSD) vs time of the N112,2O2O1-TFSI system. (a),(b),(c),(d) correspond to 298 K, 313 K, 333 K and 353 K respectively. The black horizontal dashed line indicates $\beta = 1$ and the red horizontal dashed line is the average value of beta in the selected time window. The white circles show the β values in the five time blocks.

S7.4.1 Partial conductivities

To delineate the contributions from the specific ion correlations, the total conductivity σ was divided into cation-cation σ_{++} , anion-anion σ_{--} and cation-anion σ_{+-} parts as shown below

$$\sigma = \sigma_{++} + \sigma_{--} + \sigma_{+-} \tag{S21}$$

$$\sigma_{++} = \frac{e^2}{6Vk_BT} \lim_{t\to\infty} \frac{d}{dt} \left\langle \sum_{i=1}^{N_+} \sum_{j=1}^{N_+} q_i\, q_j\, (\boldsymbol{r}_i(t) - \boldsymbol{r}_i(0)).(\boldsymbol{r}_j(t) - \boldsymbol{r}_j(0)) \right\rangle \tag{S22}$$

$$\sigma_{--} = \frac{e^2}{6Vk_BT} \lim_{t\to\infty} \frac{d}{dt} \left\langle \sum_{i=1}^{N_-} \sum_{j=1}^{N_-} q_i\, q_j\, (\boldsymbol{r}_i(t) - \boldsymbol{r}_i(0)).(\boldsymbol{r}_j(t) - \boldsymbol{r}_j(0)) \right\rangle \tag{S23}$$

$$\sigma_{+-} = \frac{e^2}{6Vk_BT} \lim_{t\to\infty} \frac{d}{dt} \left\langle 2\sum_{i=1}^{N_+} \sum_{j=1}^{N_-} q_i\, q_j\, (\boldsymbol{r}_i(t) - \boldsymbol{r}_i(0)).(\boldsymbol{r}_j(t) - \boldsymbol{r}_j(0)) \right\rangle \tag{S24}$$

where N_+ and N_- are the number of cations and anions in the simulation box respectively. Counter to our intuition, σ_{+-} contributes positively (see below) to the total conductivity implying that the oppositely charged ions are anti-correlated. Kashyap et al. showed that this peculiar behaviour is pertinent to only pure ionic liquids and is due the net momentum conservation constraint. Using the momentum conservation law, they derived relations for the partial contributions to the total conductivity. For the sake of completeness, we derive the analytical relations for σ_{++}/σ, σ_{--}/σ and σ_{+-}/σ in terms of the cation and anion masses. The derivation uses the Green-Kubo form of the ionic conductivity, which is equivalent to the Einstein formula (Eq. S19) at zero frequency,

$$\sigma = \frac{1}{3Vk_BT} \int_0^\infty \left\langle \sum_{i=1}^{N_{ion}} \sum_{j=1}^{N_{ion}} q_i\, q_j\, \boldsymbol{v}_i(t).\boldsymbol{v}_j(0) \right\rangle dt \tag{S25}$$

where $\boldsymbol{v}_i(t)$ is the center of mass velocity of ion i at time t and $\langle\rangle$ denotes the averaging

over time origins. And the partial conductivities can be written as

$$\sigma_{++} = \frac{1}{3Vk_BT}\int_0^\infty \left\langle \sum_{i=1}^{N_+}\sum_{j=1}^{N_+} q_i\, q_j\, \boldsymbol{v}_i(t).\boldsymbol{v}_j(0) \right\rangle dt \tag{S26}$$

$$\sigma_{--} = \frac{1}{3Vk_BT}\int_0^\infty \left\langle \sum_{i=1}^{N_-}\sum_{j=1}^{N_-} q_i\, q_j\, \boldsymbol{v}_i(t).\boldsymbol{v}_j(0) \right\rangle dt \tag{S27}$$

$$\sigma_{+-} = \frac{1}{3Vk_BT}\int_0^\infty \left\langle 2\sum_{i=1}^{N_+}\sum_{j=1}^{N_-} q_i\, q_j\, \boldsymbol{v}_i(t).\boldsymbol{v}_j(0) \right\rangle dt \tag{S28}$$

For the total momentum to be conserved we have,

$$m_+ \sum_{i=1}^{N_+} \boldsymbol{v}_i^+(t) = -\, m_- \sum_{i=1}^{N_-} \boldsymbol{v}_i^-(t) \tag{S29}$$

where m_+ and m_- are the masses of cation and anion respectively, $\boldsymbol{v}_i^+(t)$ and $\boldsymbol{v}_i^-(t)$ are the center of mass velocities of i^{th} cation and i^{th} anion respectively. This equation should hold at all times t.

Taking the scalar product of Eq. S29 with $\boldsymbol{v}_j^+(t_0)$, yields,

$$m_+ \sum_{i=1}^{N_+} \boldsymbol{v}_i^+(t).\boldsymbol{v}_j^+(t_0) = -\, m_- \sum_{i=1}^{N_-} \boldsymbol{v}_i^-(t).\boldsymbol{v}_j^+(t_0) \tag{S30}$$

Equation S30 holds for any j, so summing over j we get

$$m_+ \sum_{i=1}^{N_+}\sum_{j=1}^{N_+} \boldsymbol{v}_i^+(t).\boldsymbol{v}_j^+(t_0) = -\, m_- \sum_{i=1}^{N_-}\sum_{j=1}^{N_+} \boldsymbol{v}_i^-(t).\boldsymbol{v}_j^+(t_0) \tag{S31}$$

Multiplying both sides by $(q_iq_je^2)/(3Vk_BT)$ and integrating over t we get

$$\begin{aligned} &\frac{m_+}{z_+ z_+}\frac{e^2}{3Vk_BT}\int_0^\infty \left\langle \sum_{i=1}^{N_+}\sum_{j=1}^{N_+} z_+\, z_+\, \boldsymbol{v}_i^+(t).\boldsymbol{v}_j^+(t_0)\right\rangle dt \\ =& -\frac{m_-}{z_+ z_-}\frac{e^2}{3Vk_BT}\int_0^\infty \left\langle \sum_{i=1}^{N_-}\sum_{j=1}^{N_+} z_+\, z_-\, \boldsymbol{v}_i^-(t).\boldsymbol{v}_j^+(t_0)\right\rangle dt \end{aligned} \tag{S32}$$

where z_+ and z_- are the net ion charges of cations and anions respectively. Here we assume that the ionic liquid consists of only one kind of cation and one kind of anion, and all ions of the same type have the same constant net charge during the simulation. Then equation S32 reduces to

$$\frac{m_+}{z_+}\sigma_{++} = -\frac{m_-}{2z_-}\sigma_{+-} \tag{S33}$$

Similarly we can get

$$\frac{m_-}{z_-}\sigma_{--} = -\frac{m_+}{2z_+}\sigma_{+-} \tag{S34}$$

Substituting Equations S33, S34 in Equation S21 we get

$$\frac{\sigma_{+-}}{\sigma} = \frac{-2m_+m_-z_+z_-}{(m_-z_+ - m_+z_-)^2} \tag{S35}$$

$$\frac{\sigma_{++}}{\sigma} = \frac{(m_-z_-)^2}{(m_-z_+ - m_+z_-)^2} \tag{S36}$$

$$\frac{\sigma_{--}}{\sigma} = \frac{(m_+z_+)^2}{(m_-z_+ - m_+z_-)^2} \tag{S37}$$

Table S23: Partial ionic conductivity values computed from the expressions (Eq. S35,S36,S37) derived above. The masses are reported in atomic mass unit and the ionic charges in the units of elementary charge (e).

System	m_+	m_-	z_+	z_-	$\frac{\sigma_{++}}{\sigma}$	$\frac{\sigma_{--}}{\sigma}$	$\frac{\sigma_{+-}}{\sigma}$
DEME-TFSI	146.2500	280.1500	0.8024	-0.8024	0.43	0.12	0.45
$N_{112,2O2O1}$-TFSI	176.2760	280.1500	0.7640	-0.7640	0.38	0.15	0.47

Table S24: Partial ionic conductivity values of our refined force field model.

IL System	Tempera-ture (K)	σ	σ_{++}	σ_{--}	σ_{+-}	$\frac{\sigma_{++}}{\sigma}$	$\frac{\sigma_{--}}{\sigma}$	$\frac{\sigma_{+-}}{\sigma}$
DEME TFSI	298	0.244	0.105	0.029	0.110	0.43	0.12	0.45
	313	0.412	0.178	0.048	0.185	0.43	0.12	0.45
	333	0.665	0.287	0.078	0.300	0.43	0.12	0.45
	353	1.169	0.505	0.138	0.527	0.43	0.12	0.45
$N_{112,2O2O1}$ TFSI	298	0.171	0.064	0.026	0.081	0.37	0.15	0.47
	313	0.324	0.122	0.048	0.153	0.38	0.15	0.47
	333	0.619	0.233	0.092	0.293	0.38	0.15	0.47
	353	1.021	0.385	0.152	0.484	0.38	0.15	0.47

S7.4.2 Temperature dependence and activation energy

Both experimental and simulations data were fit to Arrhenius equation of the type,

$$\sigma = \sigma_0 \, exp(-E_\sigma / RT) \tag{S38}$$

where E_σ is the activation energy, σ_0 is the prefactor and R is the universal gas constant. Tables S25 and S26 list the fit parameters of DEME-TFSI and $N_{112,2O2O1}$-TFSI systems.

Table S25: Activation energy of ionic conductivity.

System	E_σ (kJ/mol)		
	Experimental	This work	Error(%)
DEME-TFSI	25.81	24.42	-5.4
$N_{112,2O2O1}$-TFSI	25.37	28.35	11.7

Table S26: Prefactor in the Arrhenius fit of ionic conductivity.

System	σ_0 (S/m)		
	Experimental	This work	Error(%)
DEME-TFSI	9267	4714	-49.1
$N_{112,2O2O1}$-TFSI	7449	16663	123.7

S7.5 Shear Viscosity

The shear viscosity was estimated using the Green-Kubo relation,[14]

$$\eta = \frac{V}{10k_BT}\int_0^\infty \left\langle \widetilde{\boldsymbol{P}}(t) : \widetilde{\boldsymbol{P}}(0) \right\rangle dt \tag{S39}$$

where $\widetilde{P}(t)$ is the symmetric and traceless part of the pressure tensor at time t and $\langle\rangle$ denotes the averaging over time origins. This formula from Evans and coworkers uses the six independent components of the pressure tensor and hence improves the statistics.[14] Due to the rapidly fluctuating nature of the pressure auto correlation function, noise gets accumulated at long times making it difficult to obtain a converged viscosity value.[15] Averaging over multiple independent trajectories is shown to have better convergence than a single long trajectory, though some ambiguity regarding the choice of converged viscosity still remains.[16,17]

Maginn and co-workers proposed a time-decomposition method in which the average (over multiple independent runs) viscosity integral is fitted to a double exponential function (Equation S40). First, the average and standard deviation of the viscosity integral were calculated. The standard deviation was then fitted to a power law (Equation S41). This power law fit was used as a weight in the fit of $\eta(t)$. To avoid the influence of long time noise on the $\eta(t)$ fit, a time cut-off t_{cut} (Equation S42) was used.

$$\eta(t) = A\alpha\,\tau_1(1 - e^{t/\tau_1}) + A(1-\alpha)\,\tau_2(1 - e^{t/\tau_2}) \tag{S40}$$

$$\sigma_\eta(t) = A\,t^b \tag{S41}$$

$$t_{cut} = t|\sigma_\eta(t) = 0.4\eta(t) \tag{S42}$$

Table S27: Shear Viscosity obtained from our refined force field model and its comparison to the corresponding experimental values.[6–8]

System	Temperature (K)	Viscosity (mPa.s)		
		Experimental	This work	Error (%)
DEME-TFSI	298	71.8	54.9 ± 6.7	-23.4
	313	37.4	29.9 ± 2.3	-19.0
	333	19.1	15.1 ± 1.1	-22.0
	353	11.4	8.9 ± 0.8	-21.5
$N_{112,2O2O1}$-TFSI	298	58.6	61.8 ± 7.8	5.2
	313	32.0	29.2 ± 2.7	-7.9
	333	17.0	14.6 ± 1.0	-11.3
	353	10.4	8.7 ± 0.7	-16.3

Table S28: Average parameters of the double exponential (Equation S40) function fit to the mean viscosity. The standard errors on the mean were obtained from the bootstrap procedure.

IL System	Tempera--ture (K)	A (GPa)	α	τ_1 (ps)	τ_2 (ps)
DEME TFSI	298	0.6649 ± 0.04	0.7702 ± 0.03	19.9 ± 4	295 ± 77
	313	0.5918 ± 0.03	0.8290 ± 0.02	16.6 ± 3	217 ± 45
	333	0.5545 ± 0.04	0.8229 ± 0.04	10.3 ± 2	107 ± 30
	353	0.5862 ± 0.09	0.8102 ± 0.05	5.6 ± 2	58 ± 25
$N_{112,2O2O1}$ TFSI	298	0.6306 ± 0.06	0.7927 ± 0.04	26.9 ± 8	375 ± 109
	313	0.6162 ± 0.06	0.8032 ± 0.04	15.3 ± 5	182 ± 56
	333	0.5870 ± 0.05	0.8399 ± 0.04	9.3 ± 3	109 ± 34
	353	0.5228 ± 0.09	0.8670 ± 0.07	7.7 ± 4	82 ± 52

S7.5.1 Temperature dependence and activation energy

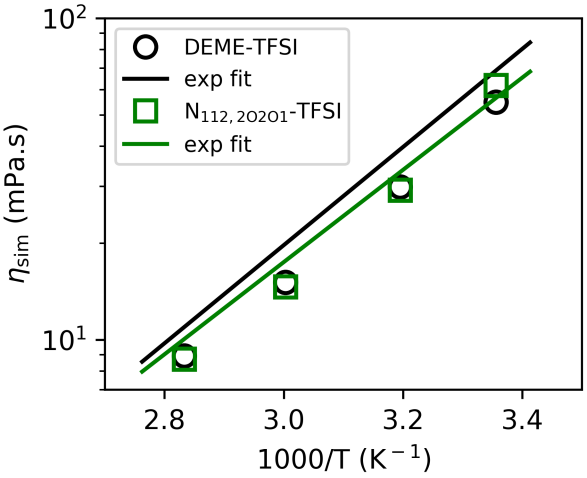

Figure S23: Viscosity vs inverse temperature of (a) DEME-TFSI system and (b) $N_{112,2O2O1}$ system. The black and the green straight lines are the Arrhenius fits to the corresponding experimental values.

Figure S23 shows the linear behaviour of viscosity (on a log-scale) with respect to inverse temperature and the close agreement with the corresponding experimental fit. Both experimental and simulations data were fit to Arrhenius equation of the type,

$$\eta = \eta_0 \, exp(E_\eta / RT) \tag{S43}$$

Table S29: Activation energy of the viscosity.

System	E_η (kJ/mol)		
	Experimental	This work	error(%)
DEME-TFSI	29.2	29.0	-0.8
$N_{112,2O2O1}$-TFSI	27.5	31.0	12.9

Table S30: Prefactor in the Arrhenius fit of viscosity.

System	η_0 (nPa.s)		
	Experimental	This work	error(%)
DEME-TFSI	518	442	-14.7
$N_{112,2O2O1}$-TFSI	866	211	-75.6

References

(1) Wang, J.; Wolf, R. M.; Caldwell, J. W.; Kollman, P. A.; Case, D. A. Development and testing of a general amber force field. *J. Comput. Chem.* **2004**, *25*, 1157–1174.

(2) Manz, T. A.; Sholl, D. S. Chemically meaningful atomic charges that reproduce the electrostatic potential in periodic and nonperiodic materials. *J. Chem. Theory Comput.* **2010**, *6*, 2455–2468.

(3) Manz, T. A.; Sholl, D. S. Improved atoms-in-molecule charge partitioning functional for simultaneously reproducing the electrostatic potential and chemical states in periodic and nonperiodic materials. *J. Chem. Theory Comput.* **2012**, *8*, 2844–2867.

(4) Iype, E.; Hütter, M.; Jansen, A. P. J.; Nedea, S. V.; Rindt, C. C. M. Parameterization of a reactive force field using a Monte Carlo algorithm. *J. Comput. Chem.* **2013**, *34*, 1143–1154.

(5) Shchygol, G.; Yakovlev, A.; Trnka, T.; van Duin, A. C. T.; Verstraelen, T. ReaxFF Parameter Optimization with Monte-Carlo and Evolutionary Algorithms: Guidelines and Insights. *J. Chem. Theory Comput.* **2019**, *15*, 6799–6812.

(6) Hayamizu, K.; Tsuzuki, S.; Seki, S. Transport and Electrochemical Properties of Three Quaternary Ammonium Ionic Liquids and Lithium Salts Doping Effects Studied by NMR Spectroscopy. *J. Chem. Eng. Data* **2014**, *59*, 1944–1954.

(7) Makino, T.; Kanakubo, M.; Umecky, T.; Suzuki, A. Electrical Conductivities, Viscosities, and Densities of N-Acetoxyethyl-N,N-dimethyl-N-ethylammonium and N,N-Dimethyl-N-ethyl-N-methoxyethoxyethylammonium Bis(trifluoromethanesulfonyl)amide and Their Nonfunctionalized Analogues. *J. Chem. Eng. Data* **2013**, *58*, 370–376.

(8) Harris, K. R.; Makino, T.; Kanakubo, M. Viscosity scaling of the self-diffusion and velocity cross-correlation coefficients of two functionalised ionic liquids and of their non-functionalized analogues. *Phys. Chem. Chem. Phys.* **2014**, *16*, 9161–9170.

(9) Araque, J. C.; Hettige, J. J.; Margulis, C. J. Modern Room Temperature Ionic Liquids, a Simple Guide to Understanding Their Structure and How It May Relate to Dynamics. *J. Phys. Chem. B* **2015**, *119*, 12727–12740.

(10) Lorch, E. Neutron diffraction by germania, silica and radiation-damaged silica glasses. *J. Phys. C Solid State Phys.* **1969**, *2*, 229–237.

(11) Allen, M.; Tildesley, D. *Computer Simulation of Liquids*; Oxford: Clarendon Pr, 1987.

(12) Yeh, I.-C.; Hummer, G. System-Size Dependence of Diffusion Coefficients and Viscosities from Molecular Dynamics Simulations with Periodic Boundary Conditions. *J. Phys. Chem. B* **2004**, *108*, 15873–15879.

(13) Kubisiak, P.; Eilmes, A. Estimates of Electrical Conductivity from Molecular Dynamics Simulations: How to Invest the Computational Effort. *J. Phys. Chem. B* **2020**, *124*, 9680–9689.

(14) Daivis, P. J.; Evans, D. J. Comparison of constant pressure and constant volume nonequilibrium simulations of sheared model decane. *J. Chem. Phys.* **1994**, *100*, 541–547.

(15) Zhang, Y.; Otani, A.; Maginn, E. J. Reliable Viscosity Calculation from Equilibrium Molecular Dynamics Simulations: A Time Decomposition Method. *J. Chem. Theory Comput.* **2015**, *11*, 3537–3546.

(16) Payal, R. S.; Balasubramanian, S.; Rudra, I.; Tandon, K.; Mahlke, I.; Doyle, D.; Cracknell, R. Shear viscosity of linear alkanes through molecular simulations: quantitative tests for n-decane and n-hexadecane. *Mol. Simul.* **2012**, *38*, 1234–1241.

(17) Mondal, A.; Balasubramanian, S. A Molecular Dynamics Study of Collective Transport Properties of Imidazolium-Based Room-Temperature Ionic Liquids. *J. Chem. Eng. Data* **2014**, *59*, 3061–3068.